

ASSESSMENT OF UNMANNED AERIAL SYSTEMS (UAS) SURVEYS IN  
DRYLAND ECOSYSTEMS: ESTIMATES OF FRACTIONAL PHOTOSYNTHETIC  
COVER AND PLANT FUNCTIONAL TYPES

by

Anna V. Roser



A thesis

submitted in partial fulfillment

of the requirements for the degree of

Master of Science in Biology

Boise State University

August 2020

© 2020

Anna V. Roser

**SOME RIGHTS RESERVED**

BOISE STATE UNIVERSITY GRADUATE COLLEGE

**DEFENSE COMMITTEE AND FINAL READING APPROVALS**

of the thesis submitted by

Anna V. Roser

Thesis Title: Assessment of Unmanned Aerial Systems (Uas) Surveys in Dryland Ecosystems: Estimates of Fractional Photosynthetic Cover and Plant Functional Types

Date of Final Oral Examination: 29 June 2020

The following individuals read and discussed the thesis submitted by student Anna V. Roser, and they evaluated their presentation and response to questions during the final oral examination. They found that the student passed the final oral examination.

Nancy F. Glenn, Ph.D. Chair, Supervisory Committee

Pat Clark, Ph.D. Member, Supervisory Committee

Trevor Caughlin, Ph.D. Member, Supervisory Committee

Marie-Anne de Graaff, Ph.D. Member, Supervisory Committee

The final reading approval of the thesis was granted by Nancy F. Glenn, Ph.D., Chair of the Supervisory Committee. The thesis was approved by the Graduate College.

## ACKNOWLEDGMENTS

I would like to thank the USDA Agriculture Research Service under Cooperative Agreement 59-2052-8-002 for funding this project, and providing resources and access to the study sites in Reynolds Creek Experimental Watershed. Thank you to my committee members for their support, advice, and feedback during this research project. Thank you to the ARS field crews for assisting with UAS flights and collecting the field data used for this project. Thank you to Josh Enterkine for help with data collection and always proposing “one more thing...”. Thank you to all members of the Boise Center Aerospace Lab, the de Graaff lab, and the Caughlin lab for your advice and camaraderie. Last, thank you to my friends and family for taking walks and providing me with support for the last two years.

## ABSTRACT

Drylands cover 41% of the global land surface and provide ecosystem services to 38% of the world's population. Dryland ecosystems have already been degraded or threatened by the increased rates of wildfire and invasive annual grasses, as well as changes in precipitation patterns. We cannot protect, mitigate, or restore drylands without comprehensive vegetation surveys. To understand ecosystem processes, we need to know the composition of vegetation at the patch and plant scales. Field observations are limited in coverage, and are expensive and time intensive. Data from Unmanned Aircraft Systems (UAS) will fill the niche between field data and medium scale remotely sensed data, and support the potential for upscaling. UAS-based remote sensing will also help extend the spatiotemporal scope of field surveys, improving efficiency and effectiveness. This study aims to test UAS methods to estimate two important vegetation metrics (1) fractional photosynthetic cover and (2) fractional cover of plant functional types.

For both objectives, a series of surveys were conducted using fine-scale spatial resolution (1-4 cm pixel<sup>-1</sup>) multispectral UAS data collected in Reynolds Creek Experimental Watershed in Southwestern Idaho, USA. Data were collected at three sites along an elevation and precipitation gradient. Each site is characterized by a different type of sagebrush: Wyoming Big Sage, Low sage, and Mountain big sage. The first study in this thesis tests multiple vegetation indices at each site to assess their accuracy in modeling photosynthetic cover. We found the Modified Soil Adjusted Vegetation index (MSAVI) had the highest accuracy when modeling photosynthetic cover at each site (62-

93%). The modeled photosynthetic cover was compared to field data consisting of point frame plots ( $n = 30$ ) at each site. Correlations between field and UAS-derived cover estimates showed significant positive relationships at the Low Sage ( $r = 0.75$ ,  $p < 0.0001$ ) and Mountain Big Sage site ( $r = 0.55$ ,  $p = 0.002$ ), but not at Wyoming Big Sage ( $r = 0.10$ ,  $p = 0.61$ ). These results demonstrate methods to estimate photosynthetic cover at fine scales in three types of sagebrush using UAS imagery. Additionally, these results suggest that UAS surveys has high correlation with field measurements at mid and high elevation sagebrush sites, but more studies are needed in low elevation sites to understand the potential of integrating UAS and field observations of photosynthetic cover.

Our second study quantified fractional cover of plant functional types in the same three sagebrush sites listed above. First, we tested Object-Based Image Analysis (OBIA) for classification of UAS surveys into plant functional types. We assessed the accuracy of the maps using confusion matrices; overall classification accuracies were strong: Wyoming Big Sage (70%), Low Sage (73%), and Mountain Big Sage (78%). The classified maps of plant functional types were compared to data from field plots ( $n = 30$ ) at each site. We found significant positive correlations for shrubs ( $r = 0.58$ ;  $0.83$ ), forbs ( $r = 0.39$ ;  $0.94$ ), and bare ground ( $r = 0.61$ ;  $0.70$ ) at our Low Sage and Mountain Big Sage. However we did not find significant relationships for the graminoid class at any site ( $r = 0.18$ ;  $0.3$ ;  $0.32$ ). Second, we tested the application of OBIA to sum shrub abundance from UAS imagery. Abundance data from field plots ( $n = 24$  per site) were tested for agreement with UAS imagery. We found no correlation at any site with field observations at the  $10\text{m}^2$  scale ( $r = -0.22$ ;  $0.12$ ;  $0.26$ ). Overall, we were able to calculate percent cover for large-unit plant functional types, such as shrubs, trees, and some forbs. Accuracy for

gramminoid classification was low due to small plant size, confounding soil reflectance, and grasses that grew beneath shrub canopies.

This research demonstrates that UAS methods can be used to estimate photosynthetic cover and map plant functional types. Using UAS surveys also increased coverage and sampling density of data when compared to traditional field observations. These findings help land managers, restoration experts, and other researchers who monitor, manage, and protect dryland ecosystems by demonstrating an accurate and less expensive approach to collecting ecosystem data.

## TABLE OF CONTENTS

ACKNOWLEDGMENTS .....	iv
ABSTRACT .....	v
LIST OF TABLES .....	x
LIST OF FIGURES .....	xii
LIST OF ABBREVIATIONS.....	xiv
INTRODUCTION .....	1
Thesis Organization .....	3
MAPPING FRACTIONAL PHOTOSYNTHETIC COVER AT FINE SPATIAL SCALES IN THREE SAGEBRUSH ECOTYPES.....	5
Introduction.....	5
Methods.....	9
Study Area .....	9
Field Data.....	14
UAS Data Collection and Processing.....	16
Assessment of Vegetation Index Accuracy and Estimation .....	17
Results.....	21
VI Assessment .....	21
Correlation with Field Data .....	22
Pixel Uncertainty .....	24
Discussion.....	26

APPLICATIONS FOR OBJECT BASED IMAGE ANALYSIS TO ESTIMATE THE FRACTIONAL COVER OF PLANT FUNCTIONAL TYPES .....	33
Introduction.....	33
Methods.....	36
Study Area .....	36
Field Data Collection .....	41
UAS Data Collection and Processing .....	42
Segmentation and Classification.....	44
Shrub Abundance.....	46
Plant Functional Type Fractional Cover .....	47
Results.....	48
Classification.....	48
Shrub Abundance.....	49
PFT Fractional Cover.....	50
Discussion.....	54
CONCLUSION.....	61
REFERENCES .....	63
APPENDIX A.....	75
APPENDIX B .....	78
APPENDIX C .....	81

## LIST OF TABLES

Table 2.1	Summary of bands from the MicaSense RedEdge 3 sensor. ....	16
Table 2.2	Details of UAS data collection at each site.....	17
Table 2.3	Spectral indices and formulas used in this study. ....	19
Table 2.4	Results from leave one out cross validation with each vegetation index at each site. The best performing indices have high average accuracies to estimate FPC and low log loss values.....	22
Table 2.5	Effect size of the strength of relationship between MSAVI values and estimation of FPC. ....	22
Table 2.6	Rho ( $r$ ) and root mean square differences calculated from UAS survey estimates of FPC and point frame field plot estimates of FPC. ....	24
Table 3.1	Summary of average shrub and herbaceous plant heights at each site. ....	40
Table 3.2	Summary of bands from the MicaSense RedEdge 3 sensor. ....	42
Table 3.3	Details of UAS data collection at each site.....	42
Table 1.4	Categories of plant functional types that were used for analysis at each site.....	44
Table 3.5	Confusion matrix for Wyoming Big Sage. ....	48
Table 3.6	Confusion matrix for Low Sage.....	49
Table 3.7	Confusion matrix for Mountain Big Sage.....	49
Table 3.8	Rho ( $r$ ) and root mean square difference for shrub abundance between UAS surveys and field observations. ....	50
Table 3.9	Summary of rho ( $r$ ) and RMSD values for each site and each correlation test for PFTs; asterisk indicate statistical significance. ....	51
Table A.1	Summary of field data correlations to estimated photosynthetic cover for each study site. ....	77

Table C.1	Segmentation Parameters used for each site on the RGB imagery within the ArcGIS Pro segmentation tool. ....	82
-----------	---	----

## LIST OF FIGURES

Figure 2.1	Annual plant functional type percent cover maps (30m) for drylands in the United States (1984-2017). Note the variability of cover in the Great Basin region (yellow). Modified from Jones et al., 2018. ....	8
Figure 2.2	Reynolds Creek watershed and location in Idaho. Modified from Nayak et al. 2010.....	10
Figure 2.3	Example of monitoring site design at Low Sage (LOS). The monitoring footprint (black) is one hectare. The point frame plots (yellow) are 1m <sup>2</sup> and the nested plots (blues) show the 10 m <sup>2</sup> , 100 m <sup>2</sup> and 400 m <sup>2</sup> squares. ....	12
Figure 2.4	Landscape photos of each site, accompanied by nadir photos over point frame plot locations. The frame is 1m <sup>2</sup> . At WBS, not the large ratio of bare ground, small bunch grasses, and large shrubs. LOS is characterized by shrubs, forbs, and grasses that are short and dense. At MBS, the shrubs are tall and there is less bare ground because there are many forbs and grasses that are dispersed rather than bunched.....	13
Figure 2.5	Point frame device at Mountain Big Sage. ....	15
Figure 2.6	Flowchart of the analytical steps taken to estimate FPC and compare ratios to field data. ....	20
Figure 2.7	Paired boxplots of the distributions of estimated FPC values for remotely sensed (blue) and field data (green) at each site. ....	23
Figure 2.8	Example of pixel values at 1m <sup>2</sup> scale (black box) at a Low Sage plot. Clockwise from the top left: True color, estimated FPC, standard deviation, and coefficient of variation. Darker pixels represent higher values. ....	26
Figure 3.1.	Examples of plant functional types in drylands. This illustration shows the canopy structure, cover, and root systems that characterize PFTs (Image from Johnson 2018 ( <a href="https://catalog.extension.oregonstate.edu/pnw714/html">https://catalog.extension.oregonstate.edu/pnw714/html</a> )). ....	34
Figure 3.2	Reynolds Creek watershed and location in Idaho. Modified from Nayak et al. 2010.....	37

Figure 3.3	Example of monitoring site design at Low Sage (LOS). The monitoring footprint (black) is one hectare. The point frame plots (yellow) are 1m <sup>2</sup> and the nested plots (blues) show the 10 m <sup>2</sup> , 100 m <sup>2</sup> and 400 m <sup>2</sup> squares. .....	38
Figure 3.4	Landscape photos of each site, accompanied by nadir photos over point frame plot locations. The frame is 1m <sup>2</sup> . At WBS, not the large ratio of bare ground, small bunch grasses, and large shrubs. LOS is characterized by shrubs, forbs, and grasses that are short and dense. At MBS, the shrubs are tall and there is less bare ground because there are many forbs and grasses that are dispersed rather than bunched.....	39
Figure 3.5	Flowchart of the analytical steps taken to classify each site to PFT, assess the classifications, and steps to estimate PFT fractional cover and shrub abundance. ....	46
Figure 3.6	Scatterplots of shrub abundance counts for each site from field and remotely sensed data. 50% and 95% Confidence Intervals are shown as blue ellipses. Note that the scales of the y axis are different for each site.	50
Figure 3.7	Boxplots of the fractional cover measured at Wyoming Big Sage for each PFT from field and remotely sensed data. ....	52
Figure 3.8	Boxplots of the fractional cover measured at LOS for each PFT from field and remotely sensed data. ....	53
Figure 3.9	Boxplots of the fractional cover measured at Mountain Big Sage for each PFT from field and remotely sensed data. ....	54

## LIST OF ABBREVIATIONS

UAS	Unmanned Aerial Systems
FPC	Fractional Photosynthetic Cover
RGB	Red Green Blue
NDVI	Normalized Differences Vegetation Index
MSAVI	Modified Soil Adjusted Vegetation Index
RCEW	Reynolds Creek Experimental Watershed
ARS	Agricultural Research Service
RTK	Real Time Kinnematic
GSD	Ground Sampling Distance
GCP	Ground Control Point
OSAVI	Optimized Soil Adjusted Vegetation Index
RMSD	Root Mean Square Difference
VI	Vegetation Index
NIR	Near Infrared
PFT	Plant Functional Type
OBIA	Object Based Image Analysis

## INTRODUCTION

Dryland ecosystems represent 41% of the global land surface and provide critical ecosystem services to 38% of the human population (Reynolds et al., 2007). For example, drylands are a buffer to desertification (Maestre et al., 2012). Drylands operate on the margins of available precipitation; this fragile balance is threatened by the incursions of human land use and climate change (Adeel et al. 2005). Invasive annual grasses and overgrazing contribute to a positive feedback loop of frequent wildfires, resulting in altered vegetation composition (Bukowski & Baker, 2013; Reisner, Grace, Pyke, & Doescher, 2013). Additionally, livestock grazing (A. G. M. Davies et al., 2016) and crop land development (Hann, Jones, Keane, Hessburg, & Gravenmier, 1998) change the landscape cover and ecosystem function. Vegetation composition in drylands is controlled by precipitation, temperature, and topography. Due to the heterogeneity of vegetation cover across small spatial scales, responses of vegetation to disturbances vary at the scale of the ecotype (Davies et al., 2016). However, responses of vegetation to a changing climate cannot be recorded without monitoring systems at the plant and plot scale because predictions of ecosystem changes must be based off of empirical data.

Additionally, it has become clear that dryland ecosystems play a large role in the global carbon cycle. Poulter et al. (2014) found that drylands account for up to 60% of interannual variability of the global carbon cycle. Plant composition and distribution affect the global carbon cycle via dynamic fluxes between the atmosphere, plants, and soil (Arora, 2002). Plant species richness and ecosystem fluxes are linked in drylands,

however it has been challenging to describe vegetation in these systems (Schaffer, Nordbotten, & Rodriguez-Iturbe, 2015; Wang, Schaffer, Yang, & Rodriguez-Iturbe, 2017). Drylands are heterogeneous over fine spatial scales, and this high spatial variation is computationally difficult to include in dynamic vegetation models of primary production so many models do not represent dryland ecosystems well (Pandit et al., 2018).

Dynamic vegetation models are used to understand the relationship between plant species and ecosystem fluxes. These models are improved by experiments and observations in the field (Leitão & Santos, 2019; Segoli, Ungar, Giladi, Arnon, & Shachak, 2012). However, the improvements are hindered by data limitations. Quantification of model parameters are needed to improve estimates of carbon stocks and fluxes into the future. Because model parameters depend on vegetation dynamics, the lack of data on the distribution and coverage of vegetation in drylands is a limitation. Data on vegetation are needed from dryland sites, including metrics like percent cover of plant functional types. Robust vegetation regime data sets will not only facilitate improved estimates of these fluxes, they will also help elucidate the impact of anthropogenic influences, including climate change, on dryland ecosystems.

The field of remote sensing is uniquely situated to fill the data gap on dryland vegetation for dynamic vegetation models. The access provided by remote sensing is crucial for studies of drylands, because they are often far from population centers which results in longer, more difficult travel to study sites (Reynolds et al., 2007). The capacity of the remote sensing community to synthesize large amounts of data is an opportunity to address complex questions of vegetation dynamics in dryland ecosystems.

Satellites can collect broad spatial datasets at high temporal frequency, which has changed the way we understand regional and global vegetation dynamics (White, Hoffman, Hargrove, & Nemani, 2005). However, it is difficult to measure sparse vegetation using sensors with coarse spatial and spectral resolution (Adão et al., 2017; A. M. Cunliffe, Brazier, & Anderson, 2016). In drylands, the high proportion of background soil or non-vascular plants confounds the noise in optical satellite remote sensing signals (Gholizadeh et al., 2018). While satellites can model and map distributions of plant cover globally, finer spatial scale data are needed to calibrate and validate these models. Due to the physical characteristics of drylands and the importance of measuring and monitoring vegetation, there is a need to develop remote sensing techniques commensurate with current field methods.

### **Thesis Organization**

This thesis contains two chapters that investigate separate questions associated with fine spatial scale remote sensing and vegetation in drylands. Both chapters assess the application of unmanned aerial systems (UAS) with a multispectral sensor to estimate plant metrics at the spatial scale of field data collection. In the first study, we began by testing vegetation indices to model fractional photosynthetic cover at peak biomass. Vegetation indices are used to increase sensitivity to vegetation features with a mathematical combination of two or more bands. To address the relationship between UAS and field data, we tested the correlation for estimates of fractional photosynthetic cover. In this study we were able to model photosynthetic cover in dryland sites at a resolution of 4cm/pixel. Our second study focuses on the importance of plant functional types in dryland ecosystems. Plant functional types are created by grouping species

together that have similar structure and function. Individual plants alter the soil texture and chemistry, and in drylands, shrubs can be especially important to plant species composition. We used object based image analysis to classify UAS imagery at the level of plant functional types. This study tested correlations between remotely sensed and field data for counts of shrub abundance and fractional cover of plant functional types. In summary, these studies can be built upon for future UAS protocols and methods for fine, spatial scale measurements of plants in drylands.

## MAPPING FRACTIONAL PHOTOSYNTHETIC COVER AT FINE SPATIAL SCALES IN THREE SAGEBRUSH ECOTYPES

### **Introduction**

Quantifying photosynthesis across scales is critically important for understanding ecosystem function. By measuring photosynthesis, we can estimate the amount of biomass produced over time. Fractional photosynthetic cover (FPC) is the amount of “green” canopy across a given area of landscape. FPC changes with the phenology of plants and the structure of the canopy. As a result, the fractional cover of photosynthesizing plants is an indicator of ecosystem function. Estimation of FPC with coverage from remote sensing data informs the parameterization of models of ecosystem functions (Lehnert et al., 2015). Measurements of FPC connect to processes in drylands, such as primary production (Seaquist, Olsson, & Ardö, 2003), desertification and erosion (Zribi et al., 2003), and hydrologic runoff (De Roo, Ooffermans, & Cremers, 1996). Other measurements that are linked to FPC include evapotranspiration (Mu, Heinsch, Zhao, M., & Running, 2007), leaf area index (Soudani, François, le Maire, Le Dantec, & Dufrêne, 2006), and the texture and albedo of the land surface (Marticorena, Bergametti, Gillette, D., & Belnap, 1997). The broad range of related processes make FPC a useful metric to obtain.

Fine-scale information on vegetation cover across large spatiotemporal extents is needed for management and for validating analyses at coarser scales. Additionally, the spatial heterogeneity of vegetation in drylands on fine scales (Figure 2.1) (de Graaff et

al., 2014) makes it difficult to transfer the UAS survey methods from one site to another, necessitating site-specific methods. Acquiring this information at adequate frequency, intensity, and extent using field-based approaches is too expensive (Gillan, Karl, Duniway, & Elaksher, 2014; Howell, Jensen, Petersen, & Larsen, 2020). As a result, there's a need to continue to develop repeatable methods for vegetation monitoring in unique dryland ecosystems. Unmanned aerial systems (UAS) offer the potential for repeated assessments of FPC at fine-scales, at numerous sites across extensive areas, all at a lower cost than field based approaches. Work from this study will potentially impact natural resource managers, policy makers, and researchers.

There are multiple examples of successful FPC quantified with remotely sensed data in ecosystems with small structural vegetation. FPC is often distinguished by “green” vs “not green” samples, referring to photosynthetically active vegetation vs. all else, i.e. soil, stems, rock, or man-made objects. Inexpensive Red Green Blue (RGB) cameras on unmanned aerial systems (UAS) can map vegetation cover in forest and near glacial landscapes (Kattenborn et al., 2020). High spatial resolution data is useful for measuring energy fluxes between plants, soils, and the atmosphere, especially when we consider how UAS data can be used for validation of satellites (Leprieur, Kerr, Mastorchio, & Meunier, 2000). With aerial imagery (2cm) over drylands, McGwire et al. (2013), were able to differentiate pixels with green cover as low as 1-10%; this finding demonstrates that the spatial scale of measurement from UAS is well suited to sparsely vegetated drylands with extremely low levels of FPC.

Studies have found that mapping and classification are more accurate with the inclusion of vegetation indices (Jiapaer, Chen, & Bao, 2011; Liu et al., 2019; Prošek &

Šímová, 2019). Vegetation indices (VIs) are mathematical combinations of wavelengths that are designed to enhance the spectral features of vegetation, and minimize confounding factors, like soil. Despite these advantages, mapping fractional photosynthetic cover in diverse rangelands can be difficult due to the heterogeneity of vegetation cover. When applied to vegetation, VIs provide a measure of vegetation vigor. Multispectral imagery allows a user to compute VIs to highlight specific features of a landscape (Hossain & Chen, 2019). While VIs are an empirical approach, they are useful because they can be related to the vegetation state and are simple to calculate. For example, researchers in Peru's dry forests used VIs like the generalized difference vegetation index to inform the segmentation of tree types from UAS imagery (Baena, Moat, Whaley, & Boyd, 2017). Peña-Barragán et al. (2011) found that VIs contributed to 90% of their models' estimations and maps of crop health and vigor. On the regional scale of the arid western U.S., the normalized vegetation index (NDVI) and the modified soil adjusted index (MSAVI) were used to separate shrubs and forest cover (Rigge et al., 2020). NDVI values from UAS imagery were used in California shrublands to create thresholds so researchers could differentiate green leaf area from non-photosynthetic cover (McGwire et al., 2013).

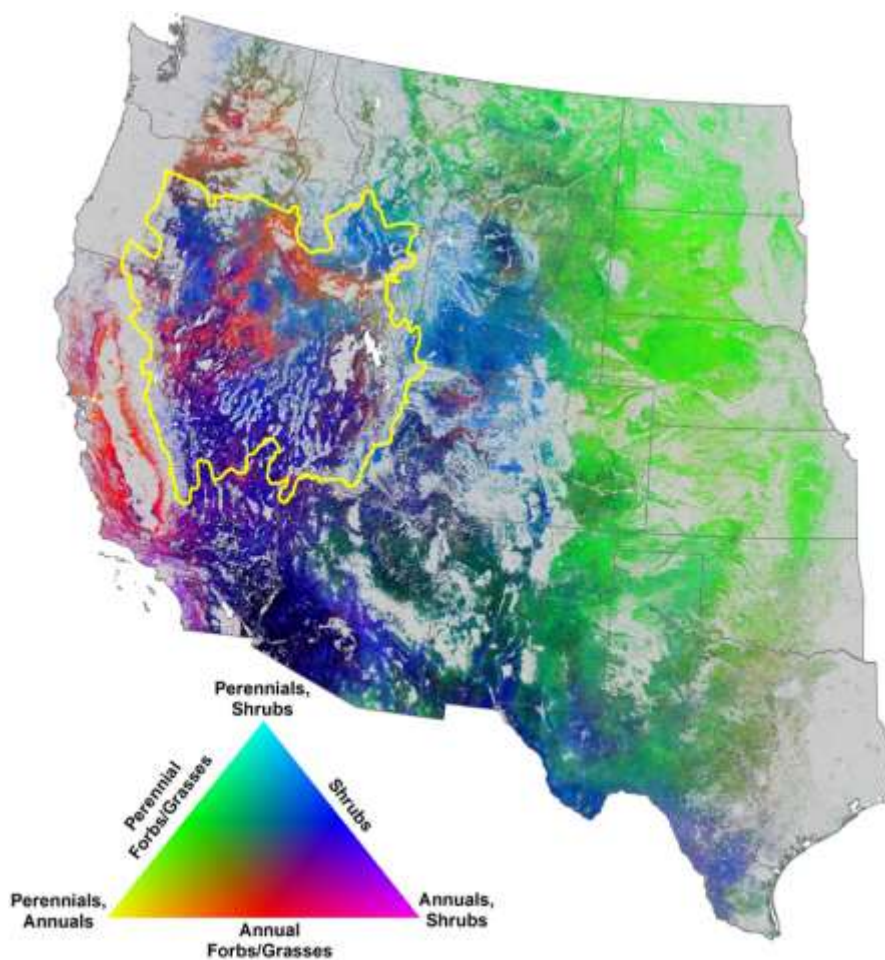


**Figure 2.1** Annual plant functional type percent cover maps (30m) for drylands in the United States (1984-2017). Note the variability of cover in the Great Basin region (yellow). Modified from Jones et al., 2018.

Reynolds Creek Experimental Watershed (RCEW), in Southwest Idaho, is an ideal study site to compare UAS methods to capture plant metrics in unique vegetation communities. Fine scale surveys of vegetation along the elevation gradient will help future campaigns collect accurate and useful information to pair with the flux tower measurements. Data in RCEW is used to infer how climate change will affect the Great Basin as a whole because the watershed is representative of the Great Basin in terms of topology, soils, vegetation, and hydrology. For example, within RCEW the predicted annual responses of gross ecosystem production and evapotranspiration to warming

temperatures will have different responses depending on the site elevation (Flerchinger et al., 2019).

The research goals of this study were to model photosynthetic cover in three types of sagebrush communities by utilizing UAS imagery. Each of the three sites is dominated by a species of sagebrush that are also common in the Great Basin: Wyoming Big Sage, Low Sage, and Mountain Big Sage. This study leverages fine spatial resolution RGB and multispectral UAS flights. We first assessed which vegetation index had the highest predictive accuracy for FPC. Additionally, we assessed the relationship between our estimates of FPC and concurrent field data. Lastly, we considered the efficacy of these methods for our study sites, as they each have unique vegetation structure and composition. Given the different characteristics of each sagebrush site, we were able to develop recommendations for UAS sampling based on the structure, density, and spectral features of each sagebrush ecotype.

## **Methods**

### Study Area

RCEW is located in Owyhee County in southwestern Idaho, USA (Figure 2.2). The 239 km<sup>2</sup> watershed has served as a natural laboratory to study dryland hydrology since 1960 (Slaughter, Marks, Flerchinger, Van Vactor, & Burgess, 2001). RCEW is 95% sagebrush steppe. The shrub communities vary across an elevation and precipitation gradient, 1101-2241m and ~230-1100mm, respectively. The watershed shares many of the same ecological characteristics with the Great Basin, a 541,727 km<sup>2</sup> region that spans the mountainous, arid west. The diverse spectrum of dryland vegetation in the Great Basin supports indicator species, including the greater sage-grouse (*Centrocercus*

*urophasianus*) (Pyke et al., 2015), and an economy of domestic livestock grazing (Knapp, 1996). Research questions about dryland management, vegetation, hydrology, and more can be addressed on a local scale in RCEW, because the watershed is a microcosm of the Great Basin.

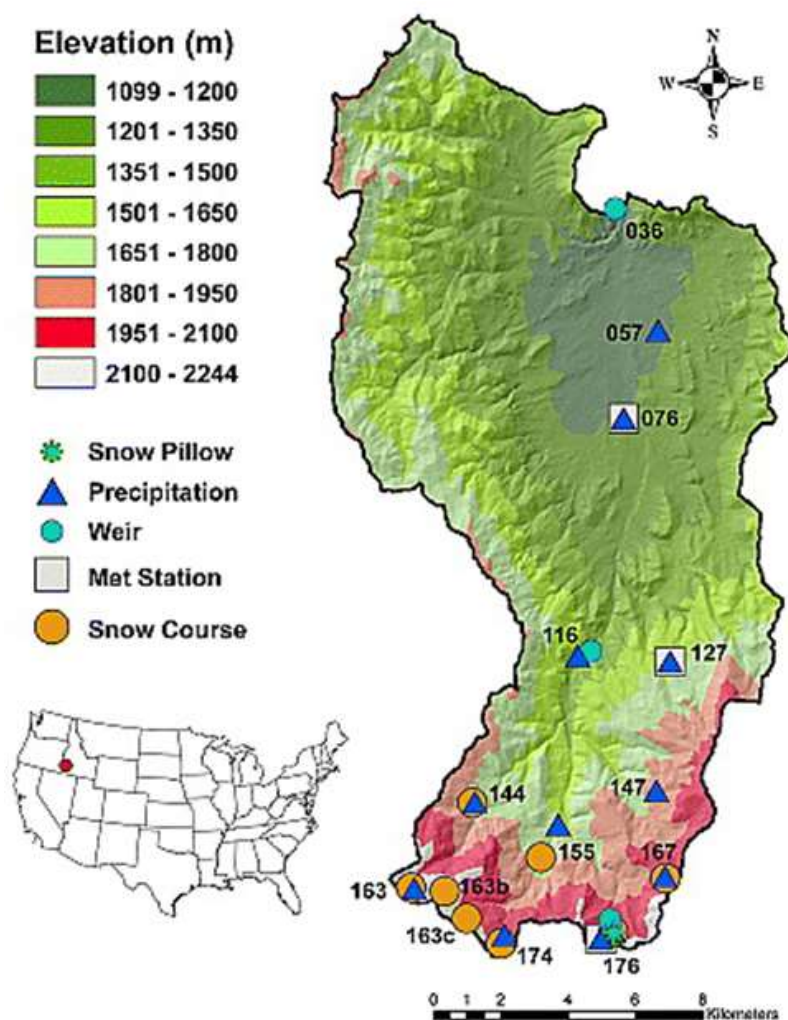


**Figure 2.2 Reynolds Creek watershed and location in Idaho. Modified from Nayak et al. 2010.**

There is a history of robust meteorologic, soil, and hydrologic data at RCEW, however vegetation surveys at the plant and plot scale on an annual basis have only recently begun. In 2015, the USDA Agricultural Research Services (ARS), began data

collection for long-term agroecosystem research of vegetation in RCEW. Plot design and methods for vegetation surveys were set up following a variation of the procedures established by the National Ecological Observatory Network (Figure 2.3). Key metrics of vegetation that are annually collected by field crews include: species abundance, species cover, and photosynthetic cover on a cm scale. There are three types of sagebrush communities here these data are collected (Figure 2.4). The study sites are named after the dominant sagebrush species present.

The first site, Wyoming Big Sage is one of the lowest sites in the watershed (1425m); on average, it receives 300mm of precipitation annually (Flerchinger et al., 2019). The average temperature is 9.4°C. The lowest site, is characterized by the presence of Wyoming big sage (*Artemisia tridentata wyomingensis*). Other shrubs include: low sage (*Artemisia arbuscula*) and yellow rabbitbrush (*Chrysothamnus viscidiflorus*). Grasses consist of Sandberg bluegrass (*Poa secunda*) and bluebunch wheatgrass (*Pseudoroegneria spicata*). Large interspaces of bare soil create an open matrix between shrubs and bunch grasses (Figure 2.4).

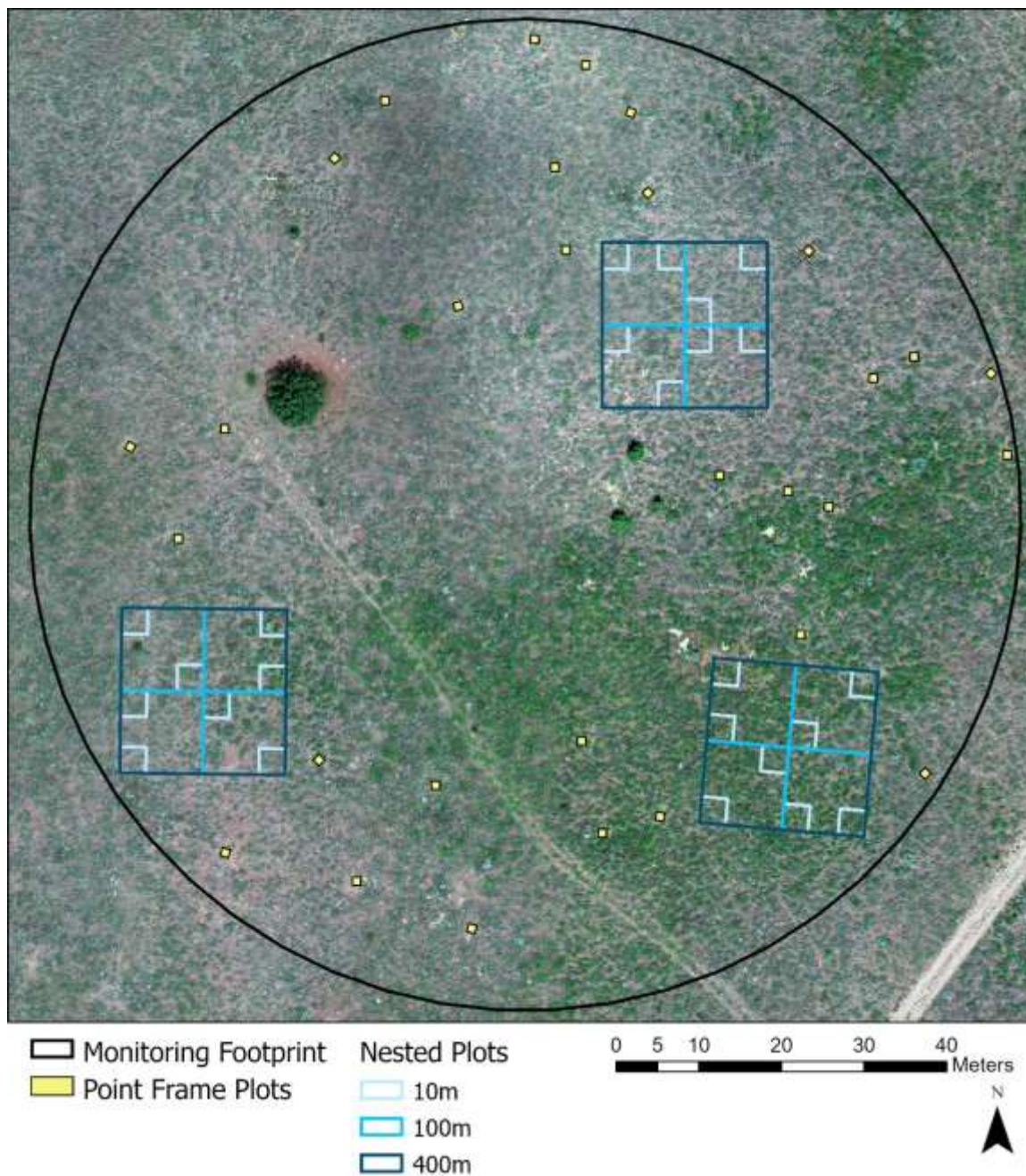


**Figure 2.3** Example of monitoring site design at Low Sage (LOS). The monitoring footprint (black) is one hectare. The point frame plots (yellow) are 1m<sup>2</sup> and the nested plots (blues) show the 10 m<sup>2</sup>, 100 m<sup>2</sup> and 400 m<sup>2</sup> squares.

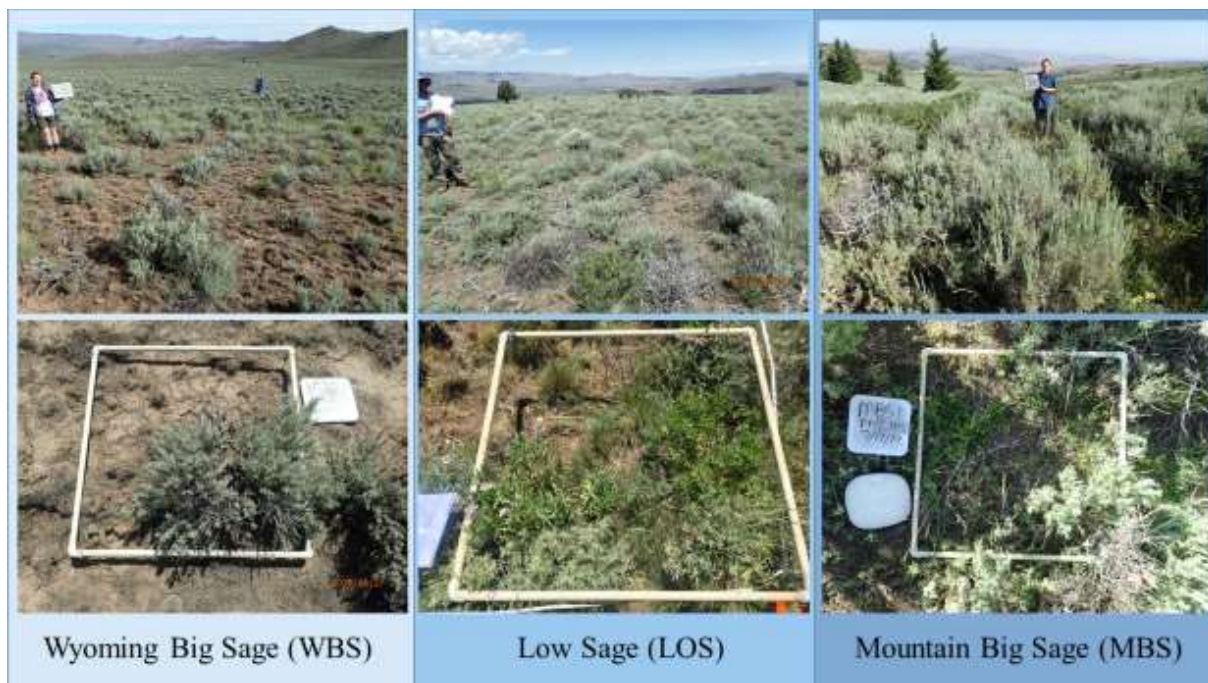


**Figure 2.4** Landscape photos of each site, accompanied by nadir photos over point frame plot locations. The frame is 1m<sup>2</sup>. At WBS, not the large ratio of bare ground, small bunch grasses, and large shrubs. LOS is characterized by shrubs, forbs, and grasses that are short and dense. At MBS, the shrubs are tall and there is less bare ground because there are many forbs and grasses that are dispersed rather than bunched.

Our second site, Low Sage, is distinct due to the short stature of the vegetation.

The Low Sage site is at 1680m, receives 335mm of precipitation annually, and the average temperature is 8.6°C. The dominant shrub at this site is low sage, with some rabbitbrush and spineless horsebrush (*Tetradymia canescens*). The low sage are interspersed with co-dominant forbs, tailcup and silvery lupine (*Lupinus caudatus* and *Lupinus argenteus*). These native forbs are nitrogen fixing plants. Most of the grasses in LOS are Sandberg bluegrass, Idaho fescue (*Festuca idahoensis*), bottlebrush squirrel tail (*Elymus elymoides*), and bluebunch wheatgrass. LOS is in the early stages of juniper (*Juniperus occidentalis*) encroachment, with several trees within the site. The amount of bare ground and interspace at LOS is relatively small with the shrubs, forbs, and grasses densely bunched together (Figure 2.4).

The third site, Mountain Big Sage, is near the top of the watershed. Mountain Big Sage is at 2110m and receives 800mm precipitation annually, over half of which is snow. The average temperature at the site is 5.6°C. The highest site has two shrub species that are co-dominant: mountain big sage (*Artemisia tridentata vaseyana*) and Utah snowberry (*Symphoricarpos oreophilus utahensis*). Lupine and other forbs such as slender cinquefoil (*Potentilla gracilis*), western yarrow (*Achillea millefolium*), and parsnipflower buckwheat (*Eriogonum heracleoides*) are common at Mountain Big Sage. The most abundant grasses are mountain brome (*Bromus marginatus*) and Kentucky bluegrass (*Poa pratensis*). This site is located near a grove of aspen (*Populus tremuloides*) and Douglas fir (*Pseudotsuga menziesii*).

In summary, these three sites vary in vegetation composition and structure, and represent common sagebrush ecotypes that are present throughout the Great Basin (Flerchinger et al., 2019).

### Field Data

During the summer of 2019, a crew of nine people collected vegetation data at each of the three sites: Wyoming Big Sage, Low Sage, and Mountain Big Sage. Each site is one hectare and has 30 point-frame or field plots (Figure 4). The field plots are 1m<sup>2</sup>, randomly dispersed throughout the hectare. The four corners of each field plot were recorded with a TopCon Real Time Kinematic (RTK) GPS. Data collected at the field plots were recorded using the point intercept method (Clark & Seyfried, 2001). The point frames are used by lowering a metal sampling pin through 20 notches along five transects (100 notches per plot). The notches are spaced 5cm apart. Every contact between the sampling pin and vegetation was recorded to species, as well the basal hit. Every contact

was also categorized as photosynthetic, “green”, or non-photosynthetic “brown”. For example, if a pin hit a sagebrush leaf that hit would be recorded as green; if the next contact with the pin was the sagebrush stem, it would be brown.

We compared several methods to calculate FPC with the point frame data; the comparisons can be found in Appendix A. The method used to calculate FPC includes all of the hits for each plot. The total number of “green” hits were summed and divided by the total number of hits in the plot. This method allowed us to normalize the ratio of FPC per plot. Additionally, using all hits to calculate FPC was most comparable to UAS data, because when light energy interacts with a sagebrush canopy, it is scattered and reflected off of multiple leaves and stems. When the UAS imagery is taken, each pixel is a mixture reflectance from leaves, stems, soil, etc., similar to the canopy hits at each point frame pin location. Field data were analyzed in R (v 3.5.2) and RStudio (v 1.2.5001).



**Figure 2.5** Point frame device at Mountain Big Sage.

## UAS Data Collection and Processing

We used a MicaSense RedEdge 3 sensor on a DJI Matrice 600 Pro. The RedEdge is a broadband multispectral sensor with bands listed in Table 2.1. We also flew a Phantom 4 with the stock RGB camera over each site (Table 2.2). All missions were planned and executed with Universal Ground Control Software (UgCS v 3.2.113). The ground sampling resolution (GSD) is not the same between the MicaSense and RGB flights for three reasons. First, the RGB flights were designed to capture  $>1\text{cm}$  GSD over the eddy covariance flux towers. As a result, the Phantom was flown at  $\sim 20\text{m}$  above ground level. These flights were completed twice: once with the camera angle at nadir and once with a  $30^\circ$  offset. The goal was to obtain a robust point cloud with structure-from-motion. For the purposes of this study, we did not include the structural information from the RGB point clouds because the flight coverage didn't include the entire vegetation monitoring footprint. Second, the MicaSense has a minimum flight altitude of  $45\text{m}$  above ground level. Below  $45\text{m}$  above ground level, images from the five MicaSense lenses will not align correctly. Lastly, we wanted complete coverage of each of the vegetation monitoring footprints with the MicaSense. At  $60\text{m}$  above ground level, we had  $>9$  images overlapping for the entire study site and we could complete the flight within the life of one battery set ( $\sim 25$  minutes).

**Table 2.1 Summary of bands from the MicaSense RedEdge 3 sensor.**

Band Number	Band Name	Center Wavelength (nm)	Bandwidth FWHM (nm)
1	Blue	475	20
2	Green	560	20
3	Red	668	10
4	Near IR	840	40
5	Red Edge	717	10

Thirteen ground control points (GCP) were placed within each study site (A. Cunliffe & Anderson, 2019). The location of all GCPs was recorded with a RTK. Each flight occurred at peak biomass over the respective study site, concurrent with field data collection. Peak biomass is determined by ARS field technicians based on the phenological state of bottlebrush squirreltail. Because the three sites are located along an elevation gradient, peak biomass occurs at different times for each site.

All UAS data were processed in Agisoft Metashape (Agisoft LLC, St. Petersburg, Russia). The processing steps were chosen with the intent to produce high quality, georeferenced orthomosaics. Multispectral photos were radiometrically calibrated. For both sensors, all photos were aligned, filtered, and exported as georeferenced orthomosaics.

**Table 2.2** Details of UAS data collection at each site.

Sensor	Wyoming Big Sage					
	GSD(cm/pixel)	AGL (m)	Reconstruction Error (cm)	Slidelap (%)	Speed (m/s)	Date
MicaSense Rededge	4.62	75	2.7	70	3	6/5/2019
RGB Phantom	0.70	20	0.7	80	6	6/4/2019
Sensor	Low Sage					
	GSD(cm/pixel)	AGL (m)	Reconstruction Error (cm)	Slidelap (%)	Speed (m/s)	Date
MicaSense Rededge	3.9	60	2.4	75	3	6/25/2019
RGB Phantom	0.9	20	0.5	80	6	6/25/2019
Sensor	Mountain Big Sage					
	GSD(cm/pixel)	AGL (m)	Reconstruction Error (cm)	Slidelap (%)	Speed (m/s)	Date
MicaSense Rededge	3.8	60	2.6	75	3	7/9/2019
RGB Phantom	0.9	20	0.5	80	6	7/2/2019

### Assessment of Vegetation Index Accuracy and Estimation

We created training and test data of photosynthetic activity using visual interpretation. We used the RGB Phantom georeferenced rasters (1cm) to create the training and test data. The RGB imagery was used to create the training and test data

because the resolution was such that we could confidently identify vegetation features. In ArcGIS Pro (v 2.5.0) we segmented each RGB raster using a mean shift algorithm. Although our end product of FPC is evaluated using pixels, we chose to use a segmentation approach for the training and test data because of the fine spatial resolution of the RGB imagery. With 1cm/pixel, plant features were split between multiple pixels. Segmentation allowed us to aggregate the spectral attributes of the multispectral imagery within each object to inform our estimation of FPC. Segmentation parameters were chosen based on the minimum plant size that we would expect to visually capture at each site. For example, Sandberg bluegrass has a basal radius of around 5cm, so segmented polygons needed to be quite small (see Appendix C for segmentation parameters for each site).

After segmentation, the author manually assigned segmented objects as “green” or “not-green”. On average, there were  $n = 2,700$  objects per site. The location of the segment objects that we sampled was determined by the location of the field plots ( $n = 30$  per site); all objects within the field plot boundaries were assigned “green” or “not-green”. The assigned segment objects were exported as polygon shapefiles.

**Table 2.3 Spectral indices and formulas used in this study.**

Vegetation Index	Acronym	Source	Equation
Normalized Difference Vegetation Index	NDVI	Rouse et al. 1974	$(\text{NIR} - \text{Red}) / (\text{NIR} + \text{Red})$
Modified Soil Adjusted Vegetation Index	MSAVI	Qi et al. 1994	$\text{NIR} + 0.5 - (0.5 * \sqrt{((2 * \text{NIR} + 1)^2 - 8 * (\text{NIR} - (2 * \text{Red})))})$
Optimized Soil Adjusted Vegetation Index	OSAVI	Rondeaux et al. 1996	$((\text{NIR} - \text{Red}) / (\text{NIR} + \text{Red} + 0.16)) * (1 + 0.16)$
Green Normalized Vegetation Index	GNDVI	Gitelson et al. 1996	$(\text{NIR} - \text{Green}) / (\text{NIR} + \text{Green})$
Normalized Difference Water Index	NDWI	McFeeters 1996	$(\text{Green} - \text{NIR}) / (\text{Green} + \text{NIR})$
Normalized Ratio Vegetation Index	NRVI	Baret 1991	$(\text{Red} / \text{NIR} - 1) / (\text{Red} / \text{NIR} + 1)$

In RStudio, we calculated multiple vegetation indices for each site (Table 2.3). We chose to test commonly used vegetation indices such as the Normalized Vegetation Index (NDVI) and the optimized soil adjusted index (OSAVI). We specifically included indices like OSAVI and the modified soil adjusted index (MSAVI) because they were designed to minimize the reflectance of bare soil (Qi et al., 1994). Our study sites have a large

amount of bare soil and vegetation with small specific leaf area which can result in a reduced sensitivity to photosynthetic cover in some indices (Leprieur et al., 2000). We overlaid the coded polygons on the stacked vegetation indices and extracted summary statistics such as mean, minimum, maximum for each polygon (Figure 2.6).

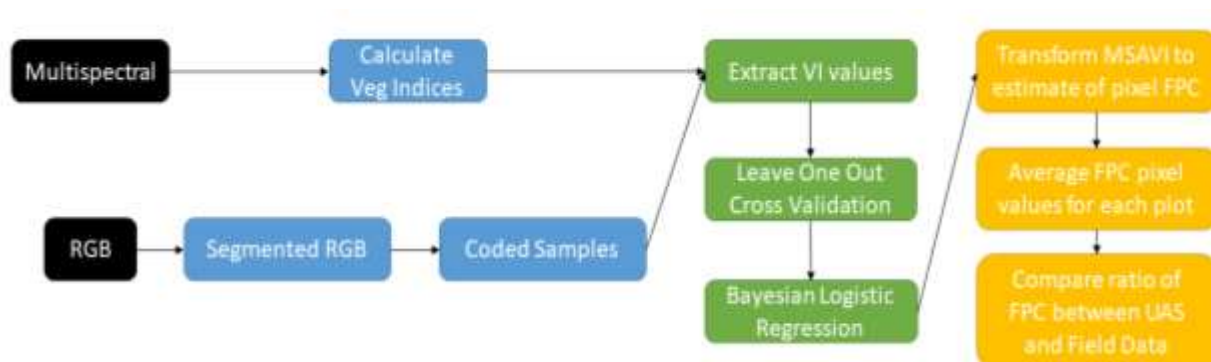


**Figure 2.6** Flowchart of the analytical steps taken to estimate FPC and compare ratios to field data.

To assess the predictive accuracy of the indices for FPC, we used a logistic regression with leave one out cross validation in RStudio. The Metrics package (Hamner and Frasco 2018) was used to iterate through each vegetation index and calculate the log loss value for each index. We compared log loss metrics and average accuracies of each index. Vegetation indices with the highest average accuracy and lowest log loss metrics were considered for predicting fractional vegetation cover.

Once the top performing vegetation index was selected, we used the rstanarm package (Goodrich et al., 2020) to run a Bayesian logistic regression to model the relationship between the samples and the vegetation index values. Default priors were used and we sampled 1000 iterations of four Markov chains after a 1000-iteration burn-in period. With the equation derived from the model, we transformed the chosen index into an estimated surface of FPC, where each pixel represents the probability of

photosynthetic cover, ranging from 0-1. We used the 4000 samples from the posterior distributions of the slope and intercept to calculate spatially explicit maps of standard deviation and the coefficient of variation.

Using the spatial boundaries of the field plots, we extracted the mean predicted FPC for each plot. We used the mean FPC values for each plot to represent the fraction of photosynthetic cover estimated across that plot. The ratio of green hits/total hits from the point frame plots served as the field derived FPC ratio per plot. We used a Pearson's correlation test to compare the FPC ratio between predicted and field data, because the values are both numeric and there was no manipulation of the independent variable. If the data were not normally distributed, we used a Spearman's Rank Sum Correlation test. We would not expect to see a perfect correlation of the point frame data and the remotely sensed data due to the differences in sampling density and methods. To quantify the differences in methods, we calculated root mean square difference (RMSD), to assess the relative difference between the field and imagery estimates of FPC.

## **Results**

### VI Assessment

Based on the leave one out cross validation, the results show that the Modified Soil Adjusted Vegetation Index had the highest estimation accuracies and lowest log loss metrics for all three sites (Table 2.4). The similarity in accuracy and log loss metrics between some VIs is notable. After rounding, MSAVI performed at the same accuracy as several other indices. Table 2.5 shows the effect size of MSAVI values to estimate FPC. We found that MSAVI values has a strong positive effect size with photosynthetic cover at all sites. We observed the strongest relationship between MSAVI and photosynthetic

cover at Mountain Big Sage (slope = 12.25), followed by Wyoming Big Sage (slope = 8.1), and then Low Sage (slope = 3.22).

**Table 2.4** Results from leave one out cross validation with each vegetation index at each site. The best performing indices have high average accuracies to estimate FPC and low log loss values.

	<b>Wyoming Big Sage</b>					
	NDVI	GNDVI	MSAVI	OSAVI	NDWI	NRVI
Average Accuracy	80.21	71.97	80.44	80.21	71.97	80.21
Logloss Metric	0.40	0.52	0.40	0.40	0.52	0.40
	<b>Low Sage</b>					
	NDVI	GNDVI	MSAVI	OSAVI	NDWI	NRVI
Average Accuracy	63.46	60.58	64.03	63.46	60.58	63.46
Logloss Metric	0.59	0.61	0.58	0.59	0.61	0.59
	<b>Mountain Big Sage</b>					
	NDVI	GNDVI	MSAVI	OSAVI	NDWI	NRVI
Average Accuracy	92.52	88.80	92.70	92.53	88.80	92.52
Logloss Metric	0.16	0.23	0.16	0.16	0.23	0.16

**Table 2.5** Effect size of the strength of relationship between MSAVI values and estimation of FPC.

	<b>Wyoming Big Sage</b>
Effect Size (95% CI)	8.098 (7.681, 8.534)
	<b>Low Sage</b>
Effect Size (95% CI)	3.22 (2.954, 3.499)
	<b>Mountain Big Sage</b>
Effect Size (95% CI)	12.25 (11.048, 13.643)

### Correlation with Field Data

When we transformed MSAVI into estimated surfaces of photosynthetic cover, we found that the estimated cover and the field data had significant, positive correlations at the middle and highest sites. At the lowest site, we found no significant correlations between the field data and estimated photosynthetic cover. The results indicate that the

estimated surfaces of photosynthetic cover from UAS Micasense data were a good match to the field data at the Low Sage and Mountain Big Sage sites.

For the lowest elevation site, we found that MSAVI had the highest predictive accuracy and lowest log loss metric (Table 2.4). When we estimated photosynthetic cover over the site and compared the FPC ratio to the field data we found a poor relationship between the data (Figure 2.7; Table 2.6). On average, the model overestimated the amount of FPC at Wyoming Big Sage by 24%. The mean FPC from field data is 25%, while the mean from the modeled FPC surface is 49%.

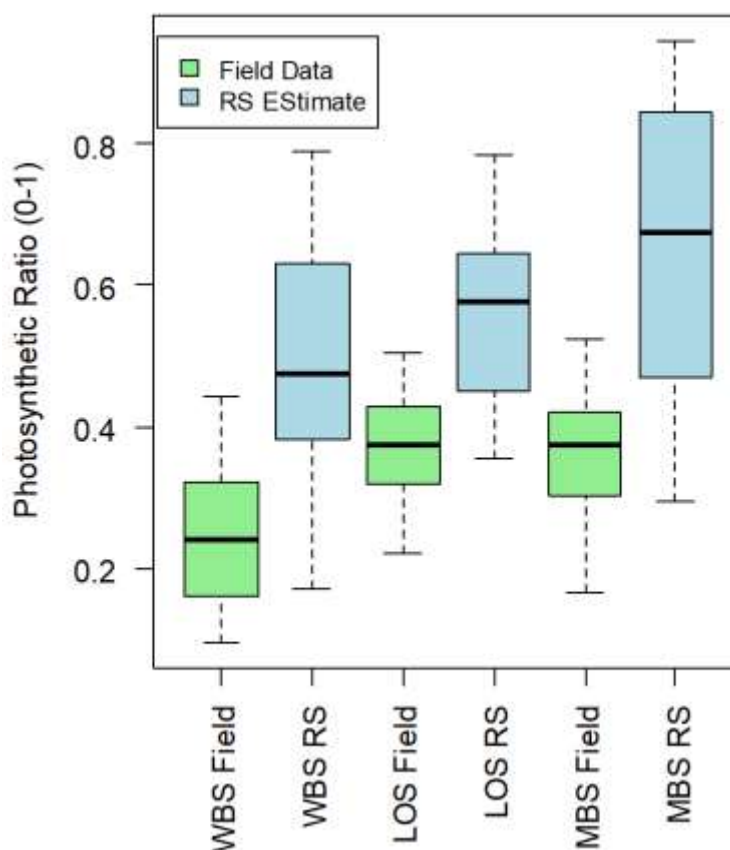


**Figure 2.7** Paired boxplots of the distributions of estimated FPC values for remotely sensed (blue) and field data (green) at each site.

**Table 2.6** Rho ( $r$ ) and root mean square differences calculated from UAS survey estimates of FPC and point frame field plot estimates of FPC.

	Wyoming Big Sage	Low Sage	Mountain Big Sage
$r$	0.1	0.75*	0.55*
RMSD	0.31	0.2	0.34

For the middle elevation site, we found that the MSAVI, had the highest predictive accuracies and lowest log loss metric. The estimated ratio of photosynthetic cover and the field data had a significant positive correlation (Figure 2.7; Table 2.6). On average, the model overestimated FPC by 18%. The mean FPC from field data is 37%, while the mean from the modeled FPC surface is 56%.

For the highest elevation site, we found that MSAVI had the highest predictive accuracy and lowest log loss metric. The estimated ratio of FPC and field ratio had a significant positive correlation (Figure 2.7; Table 2.6). On average, the model overestimated FPC by 30%. The mean FPC from field data is 36%, while the mean from the modeled FPC surface is 67%.

#### Pixel Uncertainty

We identified areas where the models performed with higher and lower uncertainty, based on the spatially explicit maps of standard deviation and coefficient of variation (Figure 6). For all sites we found the highest standard deviation and coefficient of variation values in pixels that covered man-made objects.

At Wyoming Big Sage, we found that pixels over the large, dense shrubs or completely bare soil had the lowest values of standard deviation ( $\sim 0.002$ ). Pixels over shrubs and grasses had the lowest coefficient of variation values ( $\sim 0.75$ ). Pixels with

coverage over a mixture of soil, small grasses and forbs, and litter had the highest values of standard deviation ( $\sim 0.13$ ). The highest coefficient of variation values were over areas of bare soil ( $\sim 16$ ).

Results from the Low Sage site showed a similar trend, where pixels over the dense sagebrush, lupine, and juniper had low standard deviation and coefficient of variation values. In particular, the lupine had the lowest values (standard deviation  $\sim 0.008$ , coefficient of variation  $\sim 0.8$ ). Again, we saw that pixels over bare soil, and a mixture of bare soil and small grasses and forbs, had the highest values of standard deviation and coefficient of variation (standard deviation  $\sim 0.02$ , coefficient of variation  $\sim 9$ ).

At Mountain Big Sage we observed a different pattern. The lowest values of standard deviation were pixels that covered dense shrubs and forbs, or pixels that covered the bare and mixed areas between the shrubs. The highest standard deviation values were found in pixels where the bare interspaces transitioned to shrubs or forbs ( $\sim 0.03$ ). The highest coefficient of variation values were from pixels over bare and mixed soil ( $\sim 50$ ), and man-made objects, like solar panels or fences ( $\sim 70$ ).

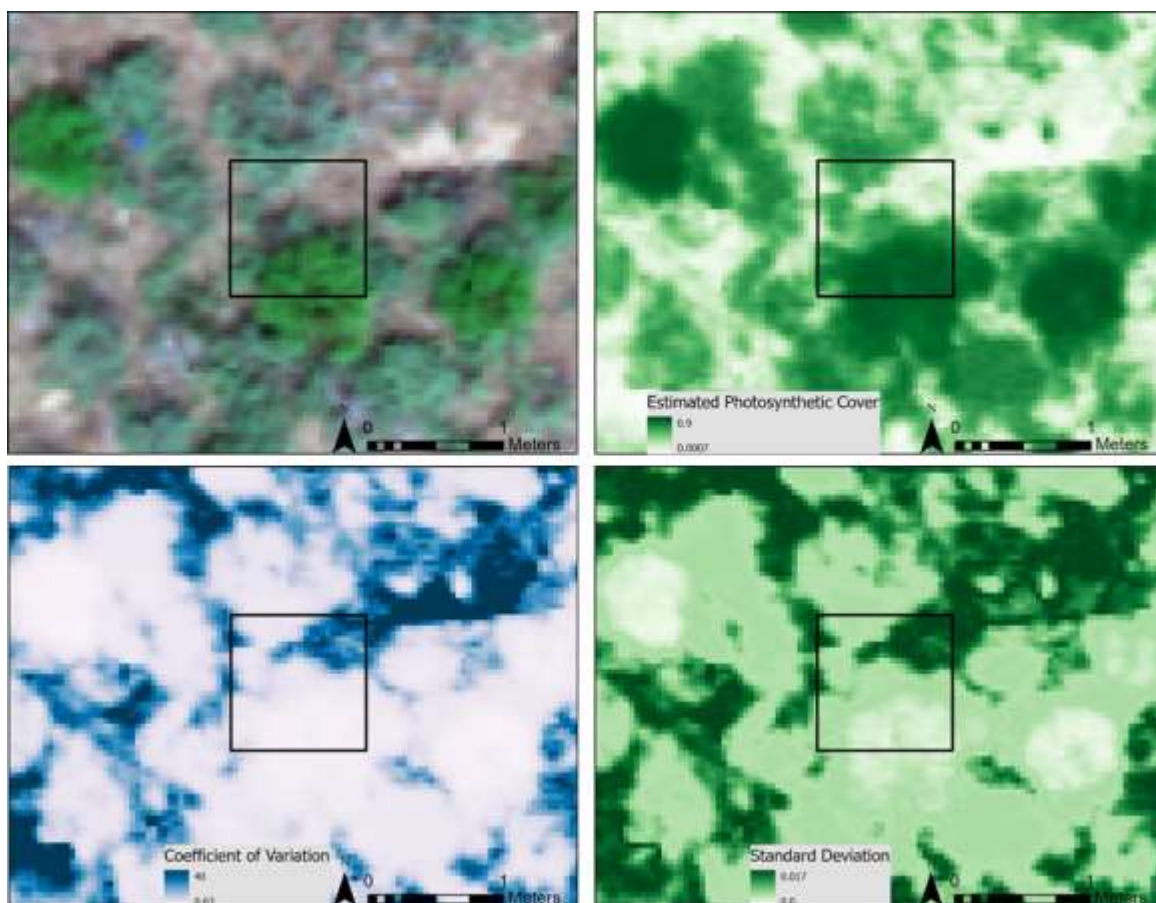


**Figure 2.8** Example of pixel values at 1m<sup>2</sup> scale (black box) at a Low Sage plot. Clockwise from the top left: True color, estimated FPC, standard deviation, and coefficient of variation. Darker pixels represent higher values.

### Discussion

Using UAS data at fine scales and applying the same processing and analytical methods throughout, we were able to estimate FPC in three sagebrush ecotypes. When we assessed the performance of vegetation indices, we found that MSAVI had the highest predictive accuracy to estimate photosynthetic cover across all three sites. These results suggest that despite the structural and composition differences of vegetation, the same UAS collection and analytical methods can be used, which is more efficient for repeat assessments of FPC across many sites. We found strong positive correlations between remote sensing and field estimates of FPC at Low Sage and Mountain Big Sage. These

results demonstrate that MSAVI has a strong functionality for estimating photosynthetic cover in semi-arid rangelands.

Although MSAVI had the highest predictive accuracy to estimate photosynthetic cover for all three sagebrush sites, NDVI was second best by hundredths of a percent (Table 2.4). This finding suggests that, if needed, NDVI could be substituted for MSAVI to estimate photosynthetic cover in Wyoming big sage, low sage, and mountain big sage dryland ecotypes. One benefit of using NDVI to estimate photosynthetic cover is that the index has been demonstrated to accurately estimate vegetation biomass and cover in diverse vegetation types across the globe (e.g., Gu et al., 2008; Horning et al., 2010).

Based on the maps of standard deviation and coefficient of variation, our models perform well over densely vegetated areas (Figure 5). This is logical, given that pixels located over dense shrubs, forbs, and grasses will record a more “pure” spectral signal. As a result, MSAVI values calculated for those pixels will have a higher probability of greenness based on our models, and lower values of standard deviation and coefficient of variation. This result agrees with the findings from Chen, Yi, Qin, & Wang (2016), where they compared field and UAS based measurements of fractional vegetation cover in Tibetan grasslands. They found more accurate model performance over areas that were more homogeneous. In our study, the small grasses and forbs in the interspaces, especially at WBS, created mixed pixels where the variance of MSAVI values was quite large. On those mixed pixels, the model estimates of photosynthetic cover are less certain. Overall, our models performed well and we were able to estimate FPC with high accuracy at pixels that we would expect to be photosynthetically active.

The model estimates of photosynthetic cover for each of our sites are higher than the field data. This result is likely due to the difference in sampling between the field and image data. The point frame measurements are limited in spatial coverage and the pin drops capture a level of detail of vegetation heterogeneity in the vertical direction that results in an underestimation of FPC similar to results from Chen et al. (2016). For example, when a sampling pin enters the canopy of a shrub, contact is recorded for leaves, stem, trunk, and any grasses, forbs or litter below the canopy. When a pixel is sampled over that same location, the information it contains is an assemblage of the reflectance and multiple scattering from the components within the pixel. This information is directly affected by the size of the pixel and the number of bands we used, and thus, our remote sensing data captures heterogeneity of FPC in a different way from the point frame method. In addition, point frame data includes the assigned photosynthetic class of each hit equally. In this study, we did not perform spectral unmixing to attribute the absolute contributions of spectral reflectance from leaves, stems, bare ground, etc., within each pixel. In contrast to using VIs, a spectral mixture analysis where spectral bands are incorporated in a model-based estimator to detect vegetation features may provide more direct correlation to vegetation structure and/or function. Notably, a hyperspectral sensor is needed to complete a successful spectral mixture analysis in drylands, and this involves more complex data collection and processing (Dashti et al., 2019). Our UAS surveys resulted in higher estimates of FPC than the field observations. We attribute this outcome to differences in measurement methods described above. MSAVI is sensitive to plant reflectance in the near infrared (NIR) portion of the electromagnetic spectrum, which highlights photosynthetically

active vegetation. Additionally, green vegetation is less likely to be underestimated because of the high sampling coverage and density of the UAS imagery. In contrast, point frame data collection has low sampling density and coverage, and is subject to user error through improper leveling, a misplaced frame, or misidentification of species.

We combined high resolution UAS imagery, segmentation, and VI values to estimate photosynthetic cover. Qualitatively, we were pleased with the surfaces of FPC for all three sites, because the pixel values accurately represented fractional green cover observed in the true color orthomosaics. FPC is a useful metric because it relates to measurements of primary production (Seaquist et al., 2003). The FPC maps that we created provide detailed spatial distribution data for future studies that relate to phenology and energy fluxes at RCEW. Additionally, we assert that these methods could be applied to other research questions. For example, researchers could map the rates of plant fungal infections by using the same methods used in this study, with the intention of estimating the likelihood of plant infection.

The FPC calculations did not correlate exactly with the point frame FPC, especially at WBS, however we did not expect them to. The value of the correlation tests is in the comparison of data collection methods. FPC surfaces inform our interpretation of the point frame data. Both methods are time intensive, either in the collection (point frame) or processing stage (UAS). And, both methods have their advantages. Point frame data are precise on the millimeter scale where the pin drops through the foliage; these types of measurements are important for canopy structure (Olsoy, Mitchell, Levia, Clark, & Glenn, 2016) and leaf area index (Clark & Seyfried, 2001), both of which relate to the biogeochemical cycle (Breda, 2003) and hydrologic interception (De Roo, Ooffermans,

& Cremers, 1996). The value of the UAS measurements are the density of data points: there are about 285 pixels/m<sup>2</sup> over 10,000 m<sup>2</sup>, compared to 100 pins/m<sup>2</sup> over 30m<sup>2</sup> total. UAS data is a product that can be combined with other GIS and raster layers for future analyses (Cagney, Cox, & Booth, 2011).

Although we treat field data as the truth, the reality is that many field collection techniques are not perfect and cannot provide a truly accurate measurement. The point intercept method to measure leaf cover is a common validation method for remotely sensed data (Cagney et al., 2011; Hillman et al., 2019; Olsoy et al., 2016). Point frames may be better suited for structural comparisons, rather than coverage. Cagney et al. (2011) found that image analysis was superior to the point-intercept method for rangeland transects because image analysis was faster, created a permanent record, and was less likely to be biased. In several instances, researchers showed that vegetation cover can be estimated more accurately with imagery than with field techniques (J. Chen et al., 2016; Rasmussen et al., 2016).

An additional benefit of a georeferenced raster was the increased spatial coverage available. Point frame plots are 1 m<sup>2</sup> and distributed within a 1 hectare site. The data from the point frames covers just 3% of a site. Although point intercept measurements provide precise data, the coverage is limited. There is an overwhelming benefit to increased spatial extent and sampling density because of linkages between remotely sensed FPC and ecosystem processes (Lehnert et al., 2015).

Our recommendations for the methods to map FPC in drylands come with some qualifications. We recognize that our results could be improved with more site replicates at each elevation. Additionally, our results would likely change had we sampled on

different days, because the data are specific to weather conditions and plant phenology. For example, at the Wyoming Big Sage site, if we had flown earlier in the summer it may have been easier to identify small forbs because they reach peak biomass earlier than squirreltail, which was our indicator for survey dates. Although we were working at a fine spatial scale, our data is still averaged at 4cm. Because some of the dryland plants are so small, our modeled surfaces of FPC cannot perfectly represent the landscape. In summary, these results must be taken under the limitations with which they were collected. On the days we sampled and with the same methods applied to each ecotype, we were able to estimate FPC at 4cm GSD for three sagebrush sites.

In the future, we think it could be beneficial to validate the estimated photosynthetic cover with a type of field data that is preferentially focused on fractional cover. One option would be to take nadir photos over the field plots. To calculate FPC from the field data (photos), SamplePoint could be used to identify and categorize plant cover within the plot (see Spaete, Glenn, & Baun, 2016 for details). Capturing one photo per plot would require much less time than taking and recording point frame measurements. That said, processing UAS imagery, troubleshooting GPS data, and running SamplePoint are also time consuming. Despite that, it is likely that automated processing steps for imagery will continue to improve in speed and ease of use, making UAS data the faster method in the future.

Based on this study, we recommend that future projects leverage the relationships between FPC, VI's, and predictive FPC surfaces with a temporal component. For this study, our sampling occurred at peak biomass for each study site. UAS flights that occurred every week or two weeks over the growing period of each study site would

capture the phenological responses of the vegetation through time. Changes in fractional photosynthetic cover over time could be linked to the measurements of eddy covariance towers in RCEW. The location of the study sites in proximity to eddy covariance flux towers is ideal to merge remotely sensed temporal measurements of FPC with GPP fluxes at the towers. Xiao et al., (2019) call for further investigation between flux tower measurements and the utilization of vegetation indices to better understand the mechanisms of the carbon cycle. This study takes a step towards that goal by testing the accuracy of multiple vegetation indices to model photosynthetic cover at three flux tower locations.

In conclusion, this study provides a comparison of UAS and field data methods to measure fractional photosynthetic cover in three types of sagebrush communities. These findings contribute to the record of vegetation data for a unique type of drylands. Despite the structural and compositional differences among our study sites, we were able to recommend MSAVI for all sites and estimate photosynthetic cover at peak biomass. The quantification of photosynthetic cover in dryland ecosystems is important to measure because of the heterogeneity of plant growth at a fine spatial scale. As drylands respond to climate change and anthropogenic development, records of vegetation growth will help us determine how these ecosystems respond to disturbances.

## APPLICATIONS FOR OBJECT BASED IMAGE ANALYSIS TO ESTIMATE THE FRACTIONAL COVER OF PLANT FUNCTIONAL TYPES

### **Introduction**

Plant functional types (PFT) are groups of species which respond in similar ways to an environment and have similar contributions to ecosystem function (López-Urrutia 2013). Examples of PFTs in drylands are graminoids, shrubs, forbs, or trees (Figure 3.1). The use of PFTs simplifies the complexity of species diversity when we try to understand the current and future roles of plant assemblages (Woodward & Cramer, 1996). Changes in abiotic factors are likely to alter the competitive relationships of dryland plant communities. As a result, monitoring at the PFT level is one of the most effective ways to quantify plant responses to environmental changes in drylands (Saiz, Le Bagousse-Pinguet, Gross, & Maestre, 2019). The physiological and chemical characteristics of PFTs affect the quality and quantity litter input (Cleveland et al., 2014; Valencia et al., 2015), as well as the distribution of nutrients and water in the soil (Prieto, Padilla, Armas, & Pugnaire, 2011). The canopy structure, size, and density of a plant impact landscape albedo (Coble & Hart, 2013).

Grouping plants by functional type assists land managers, because functional types are more generalizable to other regions and systems (Wainwright et al., 2019). There are many ways for PFTs to be applied, for example: rangeland managers want to know graminoid cover to estimate cattle forage over the grazing season (Fern, Foxley, Bruno, & Morrison, 2018). For conservationists, mapping and modeling shrub cover

provides insights on the habitat needs of native species, like pygmy rabbits (*Brachylagus idahoensis*) (Olsoy et al., 2015). Additionally, PFTs are commonly used in dynamic vegetation models to simulate changes in vegetation cover at global scales, but drylands are not well represented because of the heterogeneity of plant cover at small scales (Pandit et al., 2018). Lastly, de Graaff et al., 2014 found that changes in PFT cover are likely to result in changes to the soil carbon, nitrogen, soil organic matter, and microbial biomass. Without fine spatial scale surveys of PFTs, we cannot predict or upscale how drylands will respond to climate change. Therefore, surveys are needed to map PFTs at the scale of the plant.

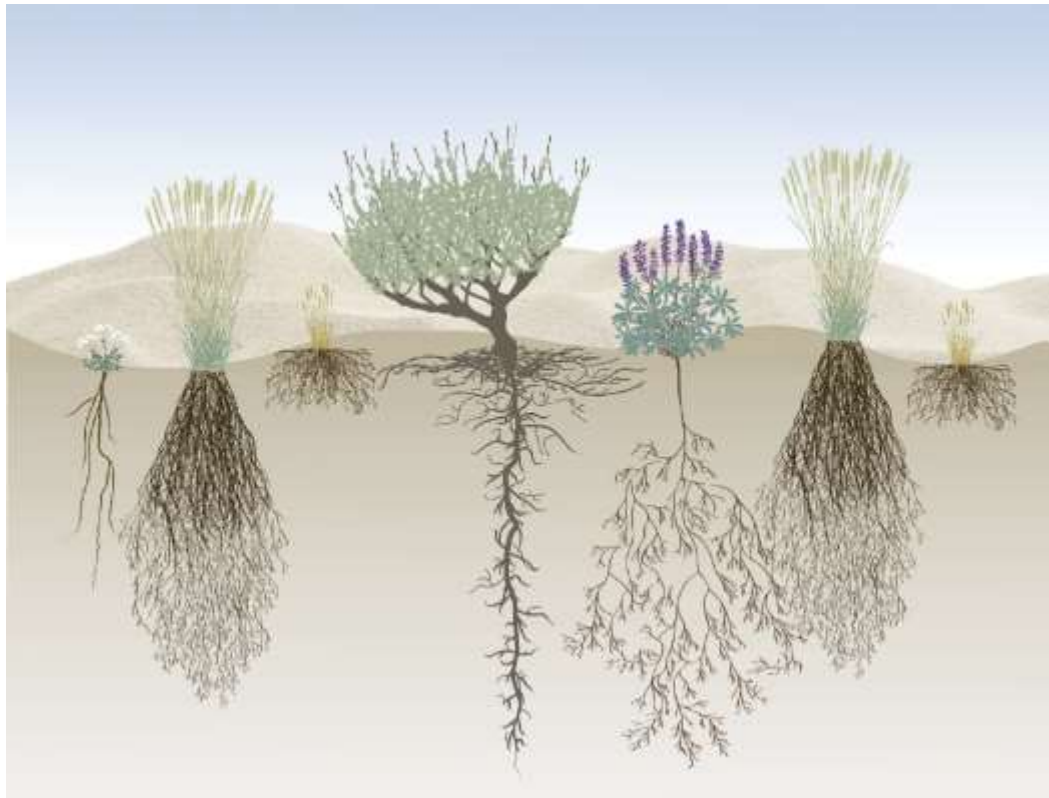


**Figure 3.1. Examples of plant functional types in drylands. This illustration shows the canopy structure, cover, and root systems that characterize PFTs (Image from Johnson 2018 (<https://catalog.extension.oregonstate.edu/pnw714/html>)).**

Applications for vegetation monitoring with unmanned aerial systems (UAS) are developing rapidly (Bestelmeyer et al., 2017). Previous studies show that UAS perform well for vegetation data collection in forested and arid environments (Wallace et al., 2012, Anderson et al., 2013, Wallace et al., 2016, Wallace, 2017). UAS are effective because they are fast, cost-efficient, and provide accurate estimates of fine scale spatial variability (Anderson et al., 2018; Olsoy et al., 2018). Estimates of vegetation coverage and bare earth area were found to be very similar for UAS images and in-situ measurements (Breckenridge & Dakins, 2011). Cagney et al. (2011) support the use of digital imagery for rangeland cover because a record of the study area is created and the imagery can be continually analyzed in future software.

Image classification analyses commonly fall into one of two approaches: pixel-based or object-based image analysis (OBIA). Supervised pixel-based analysis considers the values associated with individual pixels and categorizes them. At high spatial resolution, a square is often unrepresentative of real distributions and features of interest (Schäfer, Heiskanen, Heikinheimo, & Pellikka, 2016). Given the demonstrated need for imagery at the scale of PFTs in drylands, pixel-based image analysis alone may not be the most effective method to assess these data. OBIA differs from pixel-based classifications because thresholds and rules can be used to delineate objects like humans see them. OBIA can handle large amounts of varied remotely sensed data and automate parts of the image analysis process (Benz, Hofmann, Willhauck, Lingenfelder, & Heynen, 2004). UAS imagery provides detailed spectral, textural, and structural data, therefore it is advantageous to use OBIA. The pixel values associated with the different data layers are combined in OBIA to describe features, rather than individual pixels. In heterogeneous

shrub ecosystems, OBIA is an effective analytical method to classify vegetation types. Karl and Maurer (2010) found that OBIA was the best option for monitoring vegetation in semi-arid rangelands with fine scale UAS imagery because the technique was more accurate than pixel-based classifications.

The goals for this study were to assess the performance of OBIA classification in three types of sagebrush communities. Each of the three sites is dominated by a species of sagebrush: Wyoming Big Sage, Low Sage, and Mountain Big Sage. These three sites represent robust plots of native vegetation, defined by their location along an elevation and precipitation gradient. We had two objectives for this study. The first was to use segmentation and classification to quantify fractional cover of PFTs. Our second objective was to use the same OBIA methods to quantify shrub abundance. We implemented UAS imagery from multispectral and Red Green Blue (RGB) sensors at fine spatial scales ( $>4.5\text{cm/pixel}$ ). We assessed the efficacy of the remotely sensed methods on their own, and tested their correlation with field data collection protocols. As a result, we are able to provide recommendations for UAS collections and OBIA analysis in three distinct sagebrush ecotypes.

## **Methods**

### Study Area

This research was conducted at the Reynolds Creek Experimental Watershed (RCEW), which is located in Owyhee County in southwestern Idaho, USA (Figure 2.2). The  $239\text{km}^2$  watershed has served as a natural laboratory to study dryland hydrology since 1960 (Slaughter et al., 2001). RCEW is 95% sagebrush steppe. The shrub communities vary across an elevation and precipitation gradient, 1101-2241m and ~230-

1100mm, respectively. The watershed shares many of the same ecological characteristics with the Great Basin, a 541,727km<sup>2</sup> region that spans the mountainous, arid west. The diverse spectrum of dryland vegetation in the Great Basin supports indicator species like the greater sage-grouse (*Centrocercus urophasianus*) (Pyke et al., 2015), and an economy of domestic livestock grazing (Knapp, 1996). Research questions about dryland management, vegetation, hydrology, and more can be addressed on a local scale in RCEW, because the watershed is a microcosm of the Great Basin.

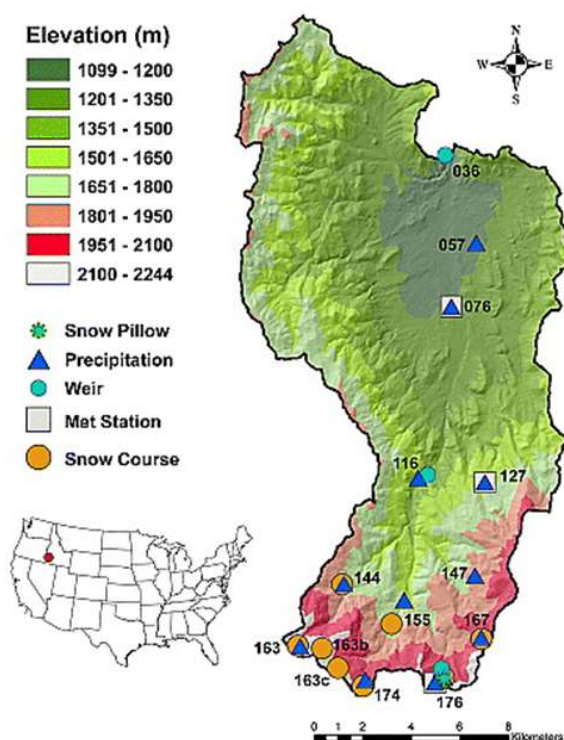


**Figure 3.2 Reynolds Creek watershed and location in Idaho. Modified from Nayak et al. 2010.**

There is a history of robust meteorologic, soil, and hydrologic data at RCEW, however a comprehensive vegetation dataset is lacking. In 2015, the USDA Agricultural Research Services (ARS), began data collection for long-term agroecosystem research of

vegetation in RCEW. Key metrics of vegetation that are annually collected by field crews include: species abundance, leaf area, and photosynthetic cover on a cm scale (Figure 3.3). There are three types of sagebrush communities (study sites) where these data are collected (Figure 3.4). The study sites are named after the dominant sagebrush species present.

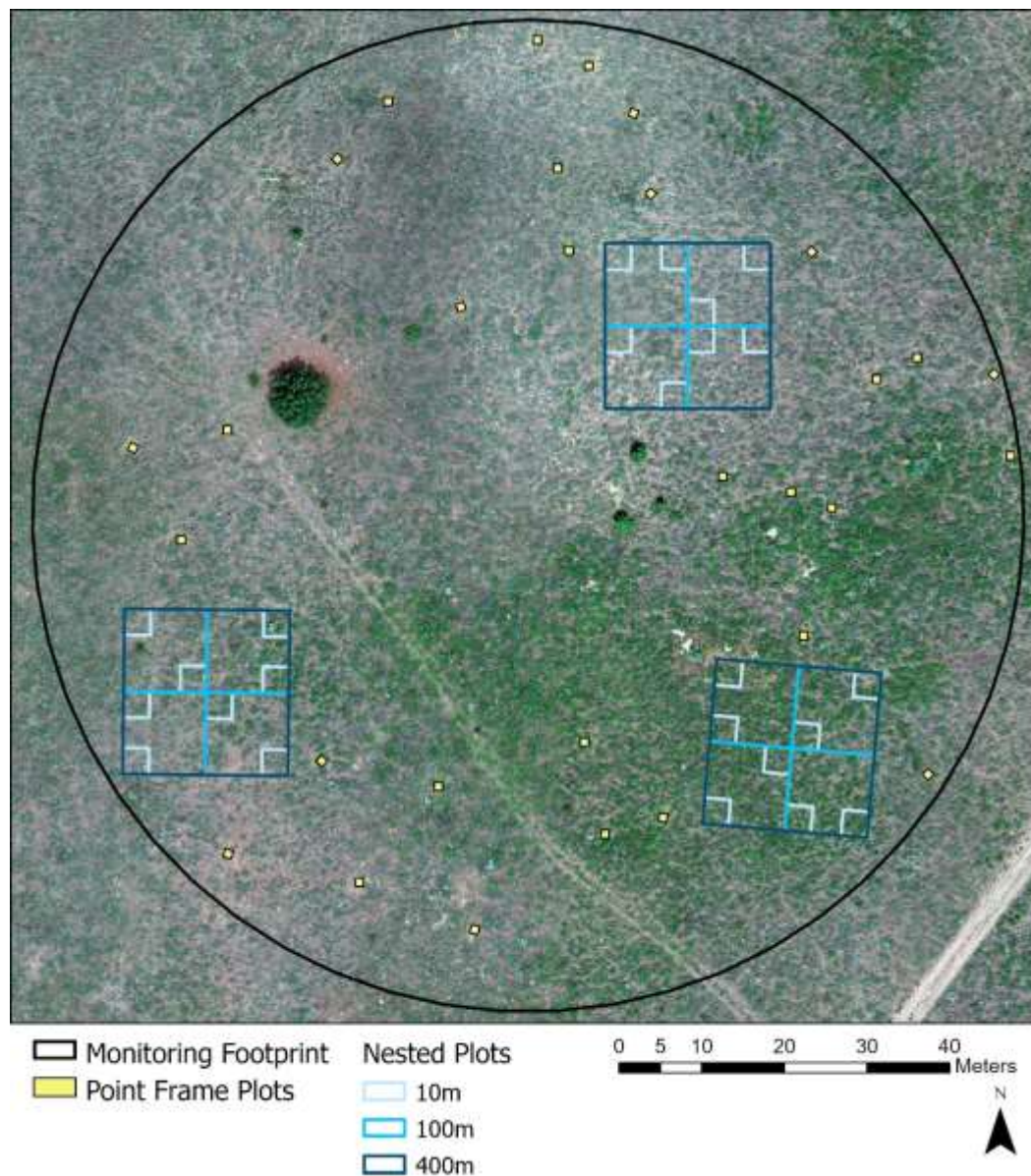


**Figure 3.3** Example of monitoring site design at Low Sage (LOS). The monitoring footprint (black) is one hectare. The point frame plots (yellow) are 1m<sup>2</sup> and the nested plots (blues) show the 10 m<sup>2</sup>, 100 m<sup>2</sup> and 400 m<sup>2</sup> squares.

The first site, Wyoming Big Sage is one of the lowest sites in the watershed (1425m); on average, it receives 300mm of precipitation annually (Flerchinger et al., 2019). The average temperature is 9.4°C. WBS, is characterized by the presence of Wyoming big sage (*Artemisia tridentata wyomingensis*). Other shrubs include: low sage (*Artemisia arbuscula*) and rabbitbrush (*Chrysothamnus viscidiflorus*). Grasses consist of Sandberg bluegrass (*Poa secunda*) and bluebunch wheatgrass (*Pseudoroegneria spicata*). The forbs at Wyoming Big Sage are relatively small with basal widths of 2-10cm and heights from 1-30cm (Table 3.1). Large interspaces of bare soil create an open matrix between shrubs and bunch grasses (Figure 3.4).

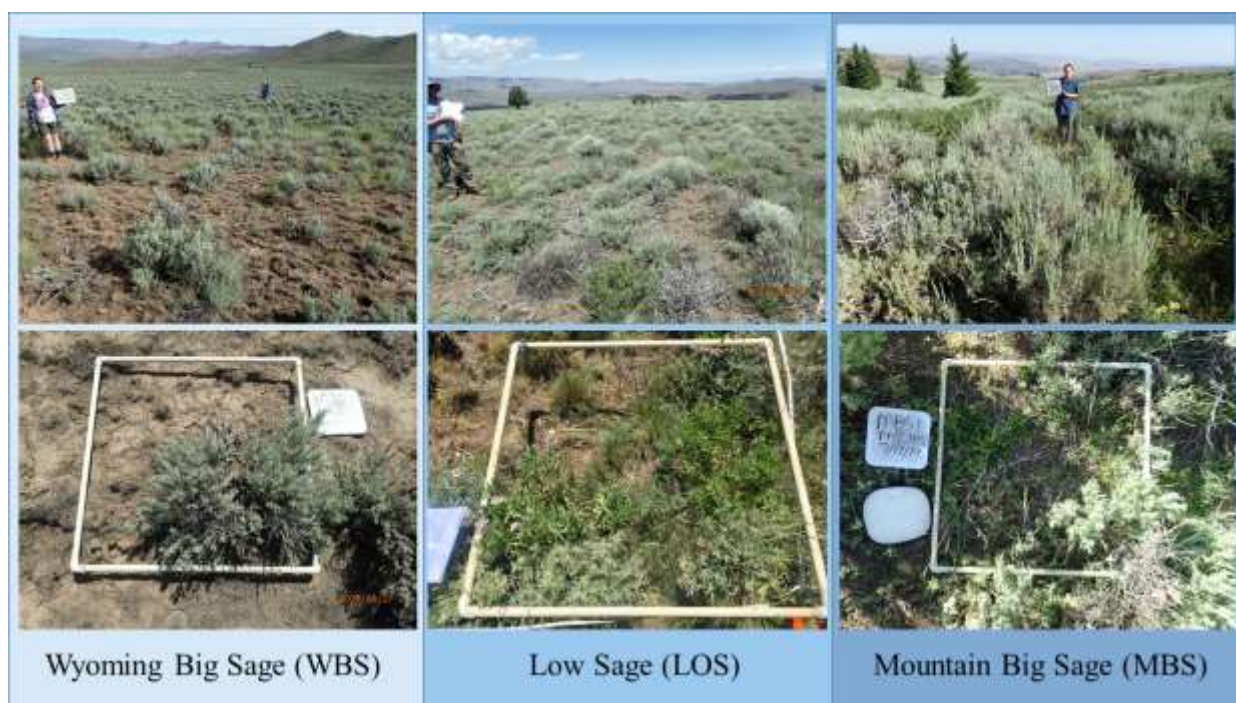


**Figure 3.4** Landscape photos of each site, accompanied by nadir photos over point frame plot locations. The frame is 1m<sup>2</sup>. At WBS, not the large ratio of bare ground, small bunch grasses, and large shrubs. LOS is characterized by shrubs, forbs, and grasses that are short and dense. At MBS, the shrubs are tall and there is less bare ground because there are many forbs and grasses that are dispersed rather than bunched.

**Table 3.1 Summary of average shrub and herbaceous plant heights at each site.**

<b>Wyoming Big Sage (WBS)</b>	
Average Herbaceous Height	11cm
Average Shrub Height	56cm
<b>Low Sage (LOS)</b>	
Average Herbaceous Height	15cm
Average Shrub Height	36cm
<b>Mountain Big Sage (MBS)</b>	
Average Herbaceous Height	15cm
Average Shrub Height	76cm

Our second site, Low Sage, is distinct due to the short stature of the vegetation. The site is at 1680m, receives 335mm of precipitation annually, and the average temperature is 8.6°C. The dominant shrub at the middle site is low sage, with some rabbitbrush and spineless horsebrush (*Tetradymia canescens*). The low sage are interspersed with co-dominant forbs, tailcup and silvery lupine (*Lupinus caudatus* and *Lupinus argenteus*). These native forbs are nitrogen fixing plants. Most of the grasses in Low Sage are Sandberg bluegrass, Idaho fescue (*Festuca idahoensis*), bottlebrush squirrel tail (*Elymus elymoides*), and bluebunch wheatgrass. Low Sage is in the early stages of juniper (*Juniperus occidentalis*) encroachment, with several trees within the site. The amount of bare ground and interspace at LOS is relatively small with the shrubs, forbs, and grasses densely bunched together (Figure 3.4).

The third site, Mountain Big Sage, is near the top of the watershed. Mountain Big Sage is at 2110m and receives 800mm precipitation annually, over half of which is snow. The average temperature at the site is 5.6°C. Two shrub species are co-dominant: mountain big sage (*Artemisia tridentata vaseyana*) and Utah snowberry (*Symphoricarpos oreophilus utahensis*). Lupine and other forbs such as slender cinquefoil (*Potentilla gracilis*), western yarrow (*Achillea millefolium*), and parsnipflower buckwheat

(*Eriogonum heracleoides*) are common at MBS. The most abundant grasses are mountain brome (*Bromus marginatus*) and Kentucky bluegrass (*Poa pratensis*). This site is located near a grove of aspen (*Populus tremuloides*) and Douglas fir (*Pseudotsuga menziesii*). In summary, these three sites vary in vegetation composition and structure. But, they all represent common sagebrush ecotypes that are present throughout the Great Basin (Flerchinger et al., 2019).

### Field Data Collection

During the summer of 2019, a crew of nine people collected vegetation data at each of the three sites: Wyoming Big Sage, Low Sage, and Mountain Big Sage. Each site is one hectare and contains three 400m<sup>2</sup> “nested” plots (Figure 3.3). Within the nested plots, plants are identified to species and presence is counted. Species density is recorded within the nested plots: grasses and forbs are counted within the 1m<sup>2</sup> sub-plots and shrubs are counted in the 10m<sup>2</sup> sub-plots. The locations of the nested plots are monumented and the locations have been recorded with a Real Time Kinematic high precision GPS (RTK). Species counts are taken once per year at approximately peak-biomass for each of the three sage communities. Peak biomass is determined by ARS field technicians based on the phenological state of bottlebrush. Because the three sites are located along an elevation gradient, peak biomass occurs at different times for each site.

Additionally, each site has 30 point-frame plots (Figure 3.3). These plots are 1m<sup>2</sup>, randomly dispersed throughout the hectare. The four corners of each field plot were recorded with a RTK. Data collected at the field plots were recorded using the point intercept method (Clark & Seyfried, 2001). The point frames are used by lowering a metal sampling pin through 20 notches along five transects (100 notches per plot). The

notches are spaced 5cm apart. Every contact between the sampling pin and vegetation was recorded to species, as well the basal hit. After the completion of field data collection, plant species were aggregated into plant functional types: shrubs, forbs, grasses, and ground in R (v 3.5.2) and RStudio (v 1.2.5001). Then the percent cover of each PFT was calculated per each point frame plot.

### UAS Data Collection and Processing

We used a MicaSense RedEdge 3 sensor on a DJI Matrice 600 Pro. The RedEdge is a broadband multispectral sensor with bands listed in Table 3.2. We also flew a standard DJI Phantom 4 over each site (Table 3.3). All missions were planned and executed with Universal Ground Control Software (UgCS v 3.2.113).

**Table 3.2 Summary of bands from the MicaSense RedEdge 3 sensor.**

Band Number	Band Name	Center Wavelength (nm)	Bandwidth FWHM (nm)
1	Blue	475	20
2	Green	560	20
3	Red	668	10
4	Near IR	840	40
5	Red Edge	717	10

**Table 3.3 Details of UAS data collection at each site.**

Sensor	Wyoming Big Sage					
	GSD(cm/pixel)	AGL (m)	Reconstruction Error (cm)	Slidelap (%)	Speed (m/s)	Date
MicaSense Rededge	4.62	75	2.7	70	3	6/5/2020
RGB Phantom	0.70	20	0.7	80	6	6/4/2020
Sensor	Low Sage					
	GSD(cm/pixel)	AGL (m)	Reconstruction Error (cm)	Slidelap (%)	Speed (m/s)	Date
MicaSense Rededge	3.9	60	2.4	75	3	6/25/2020
RGB Phantom	0.9	20	0.5	80	6	6/25/2020
Sensor	Mountain Big Sage					
	GSD(cm/pixel)	AGL (m)	Reconstruction Error (cm)	Slidelap (%)	Speed (m/s)	Date
MicaSense Rededge	3.8	60	2.6	75	3	7/9/2020
RGB Phantom	0.9	20	0.5	80	6	7/2/2020

The ground sampling resolution (GSD) is not the same between the MicaSense and RGB flights for three reasons. First, the RGB flights were designed to capture  $>1$  cm GSD over the eddy covariance flux towers. As a result, the Phantom was flown at  $\sim 20$  m above ground level. These flights were completed twice: once with the camera angle at nadir and once with a  $30^\circ$  offset. The goal was to obtain a robust point cloud with structure-from-motion. For the purposes of this study, we did not include the structural information from the RGB point clouds because the flight coverage didn't include the entire vegetation monitoring footprint. Second, the MicaSense has a minimum flight altitude of 45 m above ground level. Below 45 m above ground level, images from the five MicaSense lenses will not align correctly. Lastly, we wanted complete coverage of each of the vegetation monitoring footprints with the MicaSense. At 60 m above ground level, we had  $>9$  images overlapping for the entire study site and we could complete the flight within the life of one battery set ( $\sim 25$  minutes).

Thirteen ground control points (GCP) were placed within each study site (A. Cunliffe & Anderson, 2019). The location of all GCPs was recorded with a TopCon RTK GPS. Each flight occurred at peak biomass over the respective study site, concurrent with field data collection (Table 2). Peak biomass is determined by ARS field technicians based on the phenological state of bottlebrush squirreltail. Because the three sites are located along an elevation gradient, peak biomass occurs at different times for each site.

All UAS data were processed in Agisoft Metashape (Agisoft LLC, St. Petersburg, Russia). The processing steps were chosen with the intent to produce high quality, georeferenced orthomosaics. Multispectral photos were radiometrically

calibrated. For both sensors, all photos were aligned, filtered, and exported as georeferenced orthomosaics.

### Segmentation and Classification

We created training and test data of photosynthetic activity using visual interpretation. We used the RGB Phantom georeferenced rasters (1cm) to create the training and test data. The RGB imagery was used to create the training and test data because the resolution was such that we could confidently identify vegetation features. In ArcGIS Pro (v 2.5.0) we segmented each RGB raster. Segmentation parameters were chosen based on the minimum plant size that we would expect to visually capture at each site. For example, Sandberg bluegrass has a basal radius of around 5cm, so segmented polygons needed to be small (see Appendix C for segmentation parameters details for each site). After segmentation, the author visually identified and assigned segmented objects into PFT categories (Table 3.4). On average, there were  $n = 2,700$  objects per site. Table 3.4 only displays the PFTs that were included with correlation test with field observations. Classes such as man-made objects and shadows were also identified but are not included in the correlation tests with field observations.

**Table 1.4** Categories of plant functional types that were used for analysis at each site.

<u>Wyoming Big Sage (WBS)</u>	<u>Low Sage (LOS)</u>	<u>Mountain Big Sage (MBS)</u>
Ground	Ground	Ground
Grass	Grass	Grass
Shrub	Shrub	Shrub
	Forb	Forb
	Tree	Tree

Each study site had slightly different classes for PFTs given the unique plant community and structure at each site. At Wyoming Big Sage, the forbs are so small, that

even with 1cm/pixel imagery, we couldn't differentiate forbs from small grasses. As a result, we did not include forbs at the Wyoming Big Sage site, including only ground, grasses, and shrubs for analysis. At Low Sage, we also had difficulty identifying small forbs. The only forbs that we could identify with confidence were the silvery and tailcup lupine. The forb class is representative of lupine at Low Sage. Lastly, at Mountain Big Sage, sedge (*Carex pachystachya*) are present, however we could not differentiate them from grasses. As a result, the sedges did not receive their own class and were grouped with grasses. At the highest site, we delineated sagebrush from snowberry, however because analyses were completed at a PFT level, the species were grouped into the shrub category.

We used a random trees algorithm in ArcPro to classify the multispectral orthomosaic, using the segmentation and training (70%) and test (30%) samples from the RGB imagery. Random trees was chosen because of its resistance to overfitting and because it's compatible with segmented imagery. The segmented attributes that we included in the classification were: active chromaticity color, mean digital number, standard deviation, count of pixels, compactness, and rectangularity.

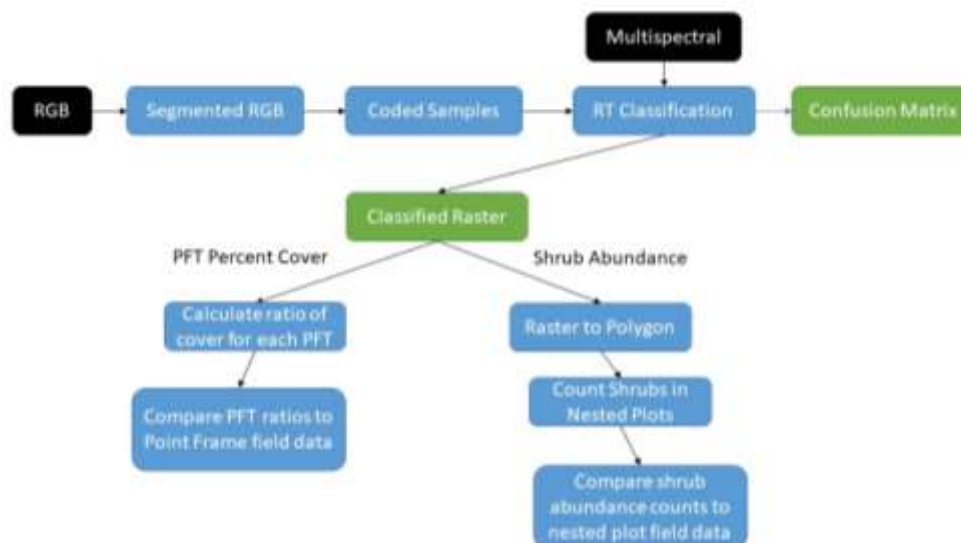


**Figure 3.5** Flowchart of the analytical steps taken to classify each site to PFT, assess the classifications, and steps to estimate PFT fractional cover and shrub abundance.

We used confusion matrices to assess the accuracy of the classified surfaces.

Confusion matrices allowed us to assess PFT classes that were correctly classified and classes where errors of commission or omission were present. The overall accuracy of each classification was calculated with the kappa coefficient. The kappa coefficient is a measure of precision because it compares whether or not classes were given the same value by the trainer and the algorithm.

### Shrub Abundance

To achieve a shrub abundance count from the remotely sensed data, we converted each classified raster into polygons. Using ArcGIS Pro select by attribute and location, we summed the number of shrub objects within the 10m<sup>2</sup> plots. Similar to the classifications completed by Baena et al. (2017), and due to the lack of positional data of all of the shrubs, we completed an accuracy assessment of plant functional type abundance at a plot level. Shrub objects were only included if their centers were inside of the plot boundary.

We used a Pearson's correlation test to compare the abundance counts at the 10m<sup>2</sup> plot level between the remotely sensed and field data, because the values are both meristic and there was no manipulation of an independent variable. If the data were not normally distributed, we used a Spearman's Rank Sum Correlation test. For each site, we calculated root mean square difference (RMSD), to assess the relative difference between the field counts and the imagery counts. Ground truth for segmentation of imagery does not exist in a way that can be assessed with an algorithm (Hossain & Chen, 2019). As a result, we chose to use RMSD as a metric of differences between the remotely sensed and field techniques, with the assumption that our field data collection is not perfect.

#### Plant Functional Type Fractional Cover

To calculate the fractional cover of each PFT, we extracted the classified raster values associated with the location of each point frame plot. By “fractional cover”, we mean the percent or ratio of active photosynthetic cover within an area of interest. We summed the number of cells associated with each cover type and calculated proportional cover for the 1m<sup>2</sup> plots.

We used a Pierson's correlation test to compare the proportional cover of each PFT at each plot between the remotely sensed and field data, because the values are both meristic and there was no manipulation of an independent variable. If the data were not normally distributed, we used a Spearman's Rank Sum Correlation test. For each site, we calculated RMSD, to assess the relative difference between the field counts and the imagery counts.

## Results

### Classification

Table 3.5 shows the classification results for Wyoming Big Sage. The overall accuracy of the PFT classification for Wyoming Big Sage was 70% and the kappa coefficient was 0.50. Notably, the errors between classes often occurred between grass and ground; these two classes display false positive and false negatives, which demonstrates the difficulty in correctly differentiating between them. The user accuracy for shrubs was 74%. Grasses had the lowest user accuracy at 20%.

**Table 3.5 Confusion matrix for Wyoming Big Sage.**

ClassName	Ground	Dead Shrubs	Man-Made	Grass	Shadow	Shrub	Total	User Accuracy	Kappa
Ground	234	3	3	20	0	3	263	0.89	
Dead Shrubs	10	15	4	2	0	0	31	0.48	
Man-Made	4	0	4	0	0	0	8	0.50	
Grass	66	0	0	20	0	14	100	0.20	
Shadow	3	0	2	0	24	0	29	0.83	
Shrub	15	1	0	2	0	52	70	0.74	
Total	332	19	13	44	24	69	0	0	
Producer Accuracy	0.70	0.79	0.31	0.45	1.00	0.75	0	0.70	
Kappa									0.50

The results for the Low Sage classification are shown in Table 3.6. The overall accuracy of the PFT classification at Low Sage was 73% and the kappa coefficient was 0.67. Similar to Wyoming Big Sage, we found that ground was often misclassified as grass. Shrubs were sometimes misclassified as grass. Lastly, forbs were often misclassified as trees. The user accuracies for bare ground and trees were high, 87% and 96%, respectively. Shrub, grass, and forb user accuracies were: 67%, 64%, and 57%, respectively.

Table 3.7 shows the classification results for Mountain Big Sage. The overall accuracy of the PFT classification for Mountain Big Sage was 78% and the kappa

coefficient was 0.72. Notable errors at this site were that forbs, shadows, and snowberry shrubs were misclassified frequently as trees. Additionally, some sagebrush was erroneously classified as ground. Almost all forbs were incorrectly classified as grass or trees. The user accuracy for sage was 62% and for snowberry it was 80%.

**Table 3.6 Confusion matrix for Low Sage.**

ClassName	Ground	Dead Shrubs	Man-Made	Forb	Grass	Shadow	Shrub	Tree	Total	User Accuracy	Kappa
Ground	104	2	10	0	2	0	2	0	120	0.87	
Dead Shrubs	4	22	2	0	2	0	1	0	31	0.71	
Man-Made	0	0	12	0	0	0	0	0	12	1.00	
Forb	1	0	0	43	3	3	4	22	76	0.57	
Grass	18	6	0	4	63	0	7	0	98	0.64	
Shadow	0	0	0	1	0	19	0	2	22	0.86	
Shrub	6	8	3	1	21	0	79	0	118	0.67	
Tree	0	0	0	0	0	1	0	23	24	0.96	
Total	133	38	27	49	91	23	93	47	501	0	
Producer Accuracy	0.78	0.58	0.44	0.88	0.69	0.83	0.85	0.49	0	0.73	
Kappa											0.67

**Table 3.7 Confusion matrix for Mountain Big Sage.**

ClassName	Ground	Dead Shrubs	Man-Made	Forb	Grass	Shadow	Snowberry	Sage	Tree	Cow-Pie	Total	User Accuracy	Kappa
Ground	173	1	1	1	2	0	1	1	0	1	181	0.96	
Dead Shrubs	11	52	4	0	0	0	0	1	0	3	71	0.73	
Man-Made	0	0	2	0	0	0	0	0	0	1	3	0.67	
Forb	2	0	0	5	30	0	0	0	22	0	59	0.16	
Grass	0	0	0	0	1	0	0	0	0	0	1	1.00	
Shadow	5	0	0	0	1	10	1	1	30	0	48	0.48	
Snowberry	0	0	0	3	1	0	83	2	15	0	104	0.80	
Sage	11	6	0	2	2	0	0	36	0	1	58	0.62	
Tree	0	0	0	1	0	0	0	0	37	0	38	0.97	
Cow-Pie	0	1	3	0	0	0	0	0	0	4	8	0.50	
Total	202	60	10	12	10	10	85	41	77	10	517	0	
Producer Accuracy	0.86	0.87	0.20	0.42	0.10	1.00	0.98	0.88	0.48	0.40	0	0.78	
Kappa													0.72

### Shrub Abundance

We found no significant relationship between shrub abundance counts at the scale of 10m<sup>2</sup> at Wyoming Big Sage, Low Sage, and Mountain Big Sage (Table 3.8). At the lowest site, the field counts and the OBIA counts an average of six and four, respectively, shrubs per plot at Wyoming Big Sage. We found no significant correlation between shrub abundance counts at the 10m<sup>2</sup> plot scale at Low Sage (Table 3.8). The OBIA counts tend

to be result in much higher abundance at both Low Sage and Mountain Big Sage than the field data (Figure 3.6). At Low Sage, the field counts for shrubs showed an average of five shrubs per plot, while the OBIA counts show an average of 15 shrubs per plot. At Mountain Big Sage, in the field, there was an average of six shrubs per plot, while the OBIA counts averaged 17 shrubs per plot.

**Table 3.8** Rho ( $r$ ) and root mean square difference for shrub abundance between UAS surveys and field observations.

	Wyoming Big Sage	Low Sage	Mountain Big Sage
$r$	0.29	-0.34	-0.17
RMSD	3.17	12.69	12.63

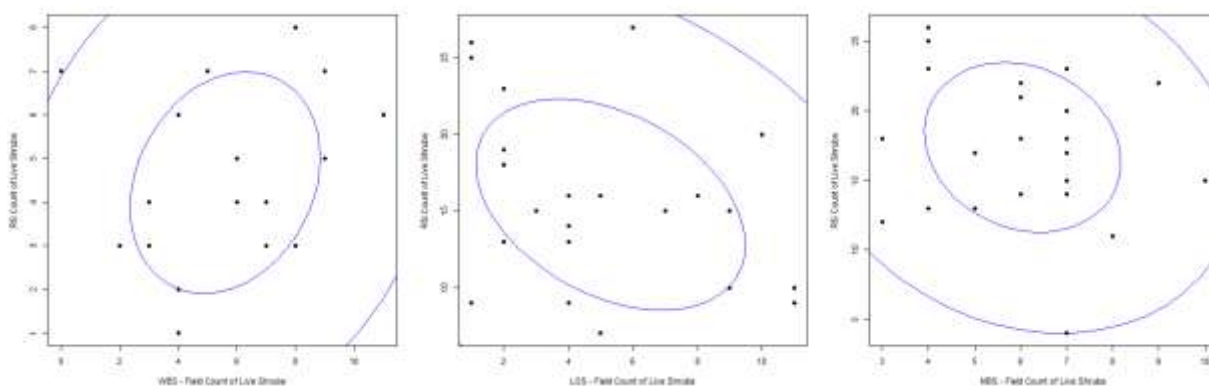


**Figure 3.6** Scatterplots of shrub abundance counts for each site from field and remotely sensed data. 50% and 95% Confidence Intervals are shown as blue ellipses. Note that the scales of the y axis are different for each site.

### PFT Fractional Cover

We found no significant correlation between PFT fractional cover at Wyoming Big Sage at the 1m<sup>2</sup> plot scale (Table 3.9). When we investigated individual functional types, we found that the distributions of fractional cover values for shrubs have a large amount of overlap (Figure 3.7). From the field data the mean fractional cover for shrubs

is 27% and the OBIA mean fractional cover is 30%. In contrast, the distributions of fractional cover values for grass had little overlap, with OBIA average cover at 5% and field measurements averaging 34%. Fractional ground cover estimates overlap, but on OBIA resulted in an average of 63%, while field data suggest an average of 34%.

**Table 3.9 Summary of rho ( $r$ ) and RMSD values for each site and each correlation test for PFTs; asterisk indicate statistical significance.**

<b>Wyoming Big Sage</b>				
	Shrubs	Grass	Ground	
$r$	0.1	0.18	0.17	
RMSD	0.32	0.32	0.4	
<b>Low Sage</b>				
	Shrubs	Grass	Ground	Forbs
$r$	0.83*	0.3	0.7*	0.94*
RMSD	0.11	0.2	0.21	0.05
<b>Mountain Big Sage</b>				
	Shrubs	Grass	Ground	Forbs
$r$	0.58*	0.32	0.61*	0.39*
RMSD	0.25	0.21	0.39	0.13

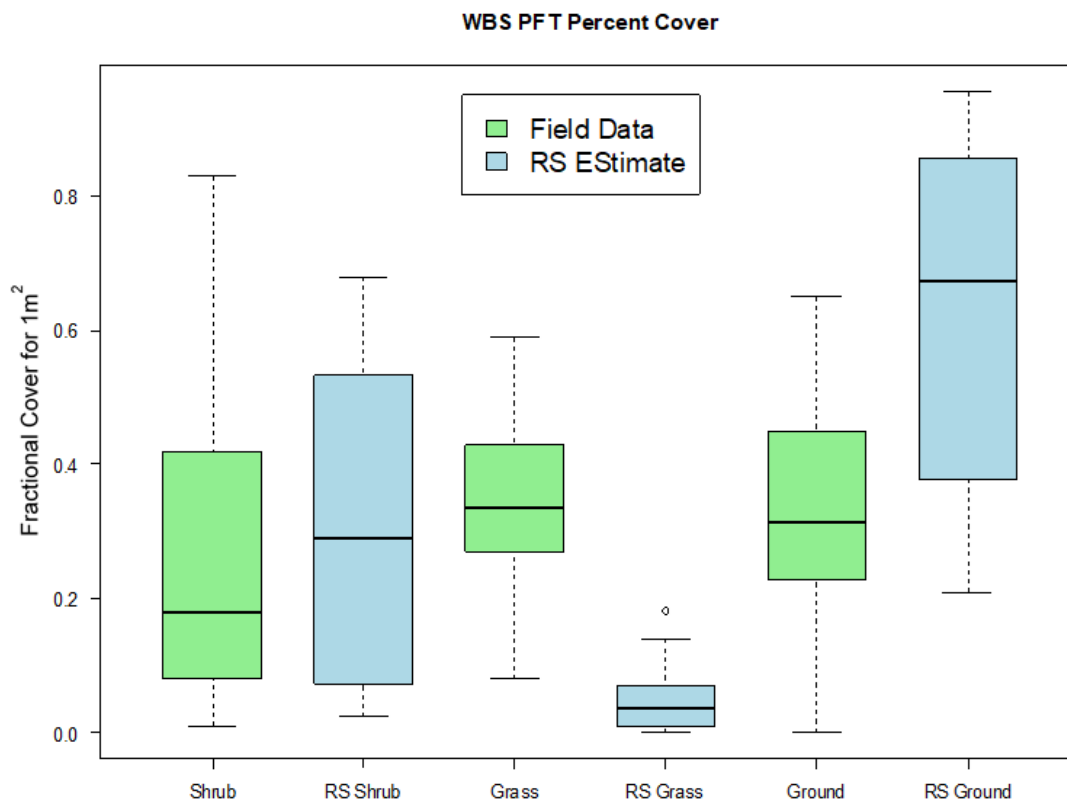


**Figure 3.7** Boxplots of the fractional cover measured at Wyoming Big Sage for each PFT from field and remotely sensed data.

At Low Sage, we found significant positive correlations between three of the four PFTs that we tested at the  $1\text{m}^2$  scale (Table 3.9). OBIA and field data measurements of fractional cover of shrubs, forbs, and ground showed positive correlations. Fractional cover for grasses did not have significant relationships. From OBIA analysis, the mean fractional cover of shrubs was 40% and from the field data it was 45% (Figure 3.8). For bare ground, the average fractional cover at  $1\text{m}^2$  scale from OBIA was 34% and 17% from the field data. The average cover for forbs was the same between the methods, at 8% and 8%, field and OBIA respectively. Similarly to Wyoming Big Sage, the average cover for grass was much higher from field data than OBIA data: 30% and 17%.

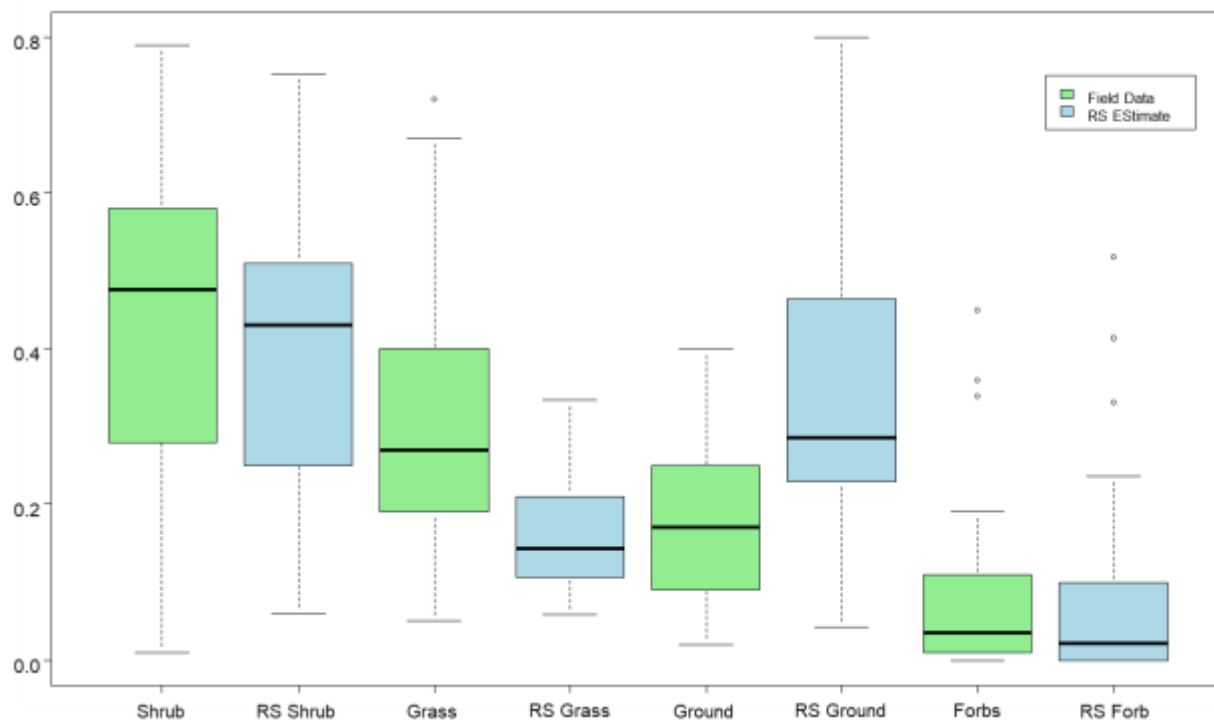


**Figure 3.8** Boxplots of the fractional cover measured at LOS for each PFT from field and remotely sensed data.

At MBS, we found significant positive correlations between three of the four PFTs that we tested at the 1m<sup>2</sup> scale (Table 3.9). OBIA and field data measurements of fractional cover of shrubs, forbs, and ground showed positive correlations. Fractional cover for grasses did not have significant relationships. We found that the fractional cover of shrubs averaged 56% from the field data and 45% from the OBIA. Although the data are positively correlated, the fractional cover averages for ground are different between the two methods: 16% from the field data and 49% from OBIA. The image analysis method overestimates fractional cover of the ground class (Figure 3.9). The average fractional cover of forbs in 1m<sup>2</sup> was low for both methods: 10% from the field data and 1% from OBIA. Finally, in a trend that we observed in all three sites, the fractional cover of grass was underestimated by OBIA; our analysis show that the average fractional cover was 18% from field data and 1% from OBIA.

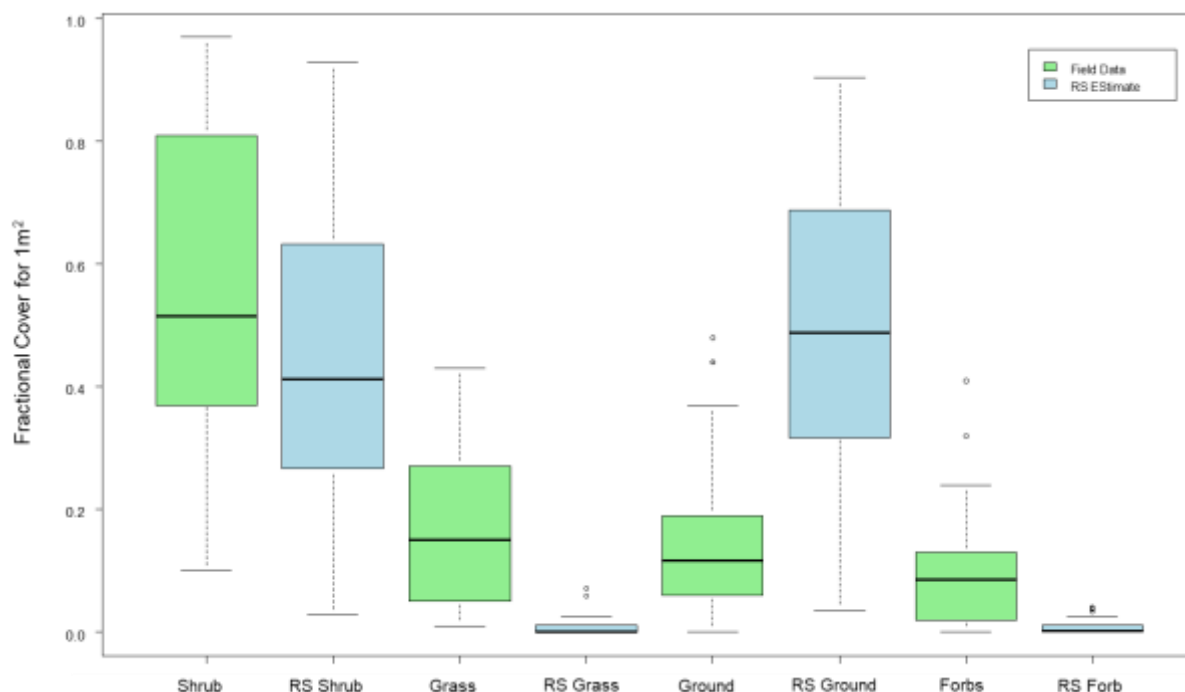


**Figure 3.9** Boxplots of the fractional cover measured at Mountain Big Sage for each PFT from field and remotely sensed data.

### Discussion

In this study, we tested the utility of using fine spatial scale UAS data to quantify PFT fractional cover and shrub abundance across three types of sagebrush ecosystems. We found that shrub abundance was not accurately estimated from remotely sensed data, given the segmentation parameters used. In the lowest elevation site, we could not confidently estimate PFT fractional cover. For mid and high elevation sites, we found strong relationships to classify and quantify PFT fractional cover at the 1m<sup>2</sup> scale. The segmentation parameters used in this study demonstrated positive results for calculating PFT fractional cover at mid and high elevation sage sites.

Our methods to use OBIA for shrub abundance counts was relatively unsuccessful, but informative for future work. One of the benefits of OBIA is the creation of features that are recognizable rather than pixelated, however many of the available

OBIA software are complicated (Hay & Castilla, 2006). Additionally, OBIA is a rapidly expanding field with a large amount of research aimed at testing and developing segmentation algorithms and parameters (Hossain & Chen, 2019). We chose to test our segmentation methods using available tools in ArcGIS Pro because of the simplicity and speed of processing. Because the tool only allows for the manipulation of spatial and spectral parameters, it's straightforward to complete segmentation quickly. Based on this, we would recommend further testing with the segmentation tool of individual shrubs because of the ease of use. However, due to the limited user input, the ArcGIS Pro segmentation tool may not be suitable for tasks which require more user knowledge or adjustment of the segmentation algorithm. If the goal of a study is to achieve abundance for multiple PFTs or species, we believe a more sophisticated segmentation algorithm is needed. Lastly, we used the same segmentation output for the shrub abundance and PFT fractional cover analyses. We opted for this method because we wanted to compare time efficient OBIA methods because a simple interface is more likely to be applied by many user groups. Given our results, we would recommend that it's worthwhile to segment for fractional cover and abundance counts separately because the overall processing time is short (less than 1hr).

At the GSD of 4cm/pixel, we found that each of the three study sites were distinct after segmentation and classification. The unique characteristics of plant size and interspace were carried through the image analysis process. However, it's unclear at what scale OBIA is most effective or if a clear answer exists; Hossain & Chen (2019) describe how a segmented feature at one scale can be homogeneous, but when viewed at a different scale it's heterogeneous. In this study we classified drylands at an fine spatial

scale and found classification accuracies similar to coarse scale studies over drylands (accuracies ~65-70%) (Homer, Aldridge, Meyer, & Schell, 2012; Rigge et al., 2020). In northern peatlands, similar in structure and fine-spatial scale heterogeneity to drylands, researchers also found that UAS classification was comparable to aerial imagery; they found that the UAS data was most valuable for training dataset construction (Räsänen & Virtanen, 2019). Coarse spatial resolution mapping from satellites provide greater coverage than achievable with UAS, however those maps cannot capture the heterogeneity at scale of ecosystem functions (Jones et al., 2018). For local management, remotely sensed data at the scale of the landscape are needed for informed decision making.

Another useful finding from this research is that even with 1cm/pixel resolution RGB imagery, some grasses and forbs could not be identified. Based on this, we question the effort to collect such fine spatial scale imagery and suggest that greater extent or more replicate sites with the multispectral sensor would be more worthwhile. This recommendation is qualified because we were not able to utilize the structural data from the 1cm imagery. Several studies have shown that the inclusion of digital surface models or canopy height models from UAS improve PFT classification accuracy (Husson, Reese, & Ecke, 2017; Komárek, Klouček, & Prošek, 2018; Sankey et al., 2018). In contrast, Prošek & Šímová (2019) found minimal improvement with the inclusion of structural information to map PFTs in shrublands. Finally, after comparing spectral and structural input to map PFTs on multiple scales, Räsänen et al. (2019) concluded that the landscape and scale of the research question determines which remotely sensed predictive variables should be included.

In our quantification of fractional PFT cover from UAS imagery, we noted several trends in our results. First, at all three sites, the OBIA fractional cover results for grass were much lower than the field data (Figures 5, 6 & 7). In tandem, we noted that all OBIA estimates of the fractional cover of ground were much higher than the field data. We present that these trends are related and likely due to the misclassification of ground and grass (Tables 4, 5 & 6). The thin structural characteristics of grasses at all three sites, make it difficult to capture via a pixel, even at a fine spatial resolution. Pixels are artificial boundaries on a landscape and their size and shape may not match all of the objects of interest (Hossain & Chen, 2019). In our study, pixel size affected the success of the classification because of the size and density of the object a pixel covered. Specifically, dense shrubs, forbs, and grasses performed well, while objects with mixed pixels with small grasses and forbs, litter, and some soil were less successful. Additionally, it's likely that pixels of grass canopy were mixed with spectral reflectance from bare ground or litter, leading to the incorrect aggregation of those grass pixels to the ground class.

Second, despite the fine spatial resolution imagery that we used to develop our training and test data, many of the forbs and grasses at our sites were too small to classify or count with confidence. This limitation is an example of the difficulty of capturing the plant community in dryland systems, where plants are structurally small or hidden near larger plants. In Portugal's dry forests, researchers were able to separate trees from the understory of shrubs, forbs, and grasses using a digital surface model (De Luca et al., 2019). It's likely that the inclusion of structural information would improve the separation of PFTs. Forsmoo et al. (2018) were able to accurately estimate the height of a

small rye grass and clover, however this required a GSD of ~0.5cm and three flights over the same study site. Based on other studies in sagebrush sites, 3cm resolution imagery is not fine enough to capture structural information from small grasses and forbs (Gillan et al., 2014). Structural information may be useful if it can discriminate small grasses and forbs from terrain and litter surface background. Further investigation is needed to develop methods capable of identifying and mapping these small spatial scale plants.

Third, when compared among the sites, the methods presented in this study were the most accurate for the Low Sage site. We found strong positive correlations between nearly all PFTs tested at this site. We partially attribute the success of the methods at Low Sage to the inherent physical properties of the plant community. The shrubs, grasses, and forbs at the middle site are all relatively short and dense (Table 1). In contrast to the other sites, the shrubs at Low Sage are so short that there are few forbs and grasses that grow beneath them – there is little to no understory. As a result, the segmentation and classification steps at the Low Sage site correctly identify PFTs because the plants grow at about the same height.

Although we also found positive correlations between the field and remotely sensed estimations of PFT fractional cover at Mountain Big Sage, the relationships were not as strong as Low Sage. Forbs and grasses were quite difficult to identify from the 1cm/pixel imagery. Grasses at Mountain Big Sage grow close and into the canopies of sage and snowberry. Additionally forbs were under estimated because they also grow near shrub canopies or were misclassified as grass or trees. We would expect that the inclusion of structural information would reduce the misclassification of forbs as trees.

Based on our findings for quantifying PFT fractional cover, we would recommend applying segmentation and classification to track the changes in fractional cover over a growing season and through multiple years. In our study, we used data from only one UAS flight at each site. Classification results would likely be different if we had UAS imagery from throughout the growing season, as multiple studies have shown improvements in classification accuracy (B. Chen, Huang, & Xu, 2017; Dudley, Dennison, Roth, Roberts, & Coates, 2015; Lu et al., 2017). Plants have different phenological cycles that result in different dates for ‘green-up’ and peak biomass, therefore the inclusion of imagery through time provides another layer of information to identify different vegetation classes. Additionally, it’s likely the inclusion of other data types, such as structure-from-motion point clouds or hyperspectral imagery, would improve our results (Husson et al., 2017; Räsänen & Virtanen, 2019). However, inclusion of hyperspectral data collection and processing for each site would have greatly increased the analysis workload (Palace et al., 2018).

The maps of PFT for these sage sites can be related to questions about dryland ecosystem processes. When we consider the importance of woody shrubs as islands of fertility (Ochoa-Hueso et al., 2018), PFT maps could be used to monitor shrub cover over time and the herbaceous diversity in the surrounding area. These maps could also be paired with soil and microbial sampling regimes because PFTs have an impact on the microbial community (de Graaff et al., 2014), as well as soil texture (Prieto et al., 2011). Soil samples associated with known PFT locations would allow for the creation of an interpolated map of the microbial community. Finally, the relative litter inputs from different PFTs have an effect on the carbon cycle (de Graaff et al., 2014; Valencia et al.,

2015), therefore PFT maps could be used to estimate the relative proportion of litter input over a much larger area than field sampling.

Changes in average temperature and precipitation patterns are likely to affect the plant communities in the sagebrush steppe. An application of these methods over the course of multiple growing seasons would greatly expand the record of data available to track and analyze potential changes in the plant communities over time. Specifically, mapping PFT fractional cover over time will allow us to quantify the relative cover of PFTs through the growing season.

## CONCLUSION

Across the western United States, we've already lost one half of the native sagebrush steppe to a combination of land use/land change and climate change (K. W. Davies et al., 2011). There's an urgent need to protect and sustainably manage dryland ecosystems – baseline surveys are needed to record trends and responses of vegetation. These data can inform dynamic vegetation models to predict gross primary production, a key metric to gauge if drylands will be carbon sources or sinks in the future. Remotely sensed data, commensurate with field surveys and measurements, helps us link fine scale measurements to vegetation dynamics at regional scales. To address the challenges of data collection in drylands, we tested the efficiency and accuracy of UAS surveys in three types of sagebrush and how they performed compared to field observations. We found that MSAVI could be used to estimate fractional photosynthetic cover at Wyoming Big Sage, Low Sage, and Mountain Big Sage sites. Additionally, we were able to map plant functional types at Low Sage and Mountain Big Sage. In both studies, correlations between UAS surveys and field observations were highest at Low Sage and Mountain Big Sage sites, and lowest at Wyoming Big Sage.

In the first study, we focused on fractional photosynthetic cover (FPC). For all three sites, we found that Modified Soil Adjusted Vegetation Index was the most suitable vegetation index to model FPC. We compared the modeled surfaces to FPC from point frame field plots. The measurements showed significant positive correlations at the Low Sage and Mountain Big Sage sites. We also found that the remotely sensed estimates

were consistently higher than the field data. Overall, this study demonstrates how UAS imagery can be used to model FPC at fine spatial scale resolution, with coverage and sampling density that greatly exceeds field data. Wyoming Big Sage has large patches of soil interspace and small forbs and grasses – these characteristics resulted in poor relationships between UAS surveys and field observations. We recommend further investigation to accurately map fractional photosynthetic cover in sparsely vegetated sagebrush ecosystems.

In our second study, our goals were centered on PFTs. We used OBIA to calculate shrub abundance and to estimate PFT fractional cover. The methods tested for PFT fractional cover were successful in terms of classification, at all sites. We found significant positive correlations for PFT fractional cover between UAS and field data at mid and high elevations. Further testing of OBIA methods in Wyoming Big Sage sites is needed to improve estimates of PFT cover and photosynthetic activity. This research is all the more important because low elevation sagebrush ecotypes are the most likely to be invaded by annual grasses (K. W. Davies et al., 2011) and the least likely to recover after wildfires (Wainwright et al., 2019). Lastly, linking the PFT maps with the surfaces of FPC will allow us to estimate the relative contributions of plant functional types of gross primary production fluxes over the course of the year.

We recommend continued inclusion of UAS with field surveys because of the increased coverage and the number of different analyses that can be applied to the same imagery. In conclusion, these results show that UAS image analysis can be successfully completed at the same scale as field data in drylands.

## REFERENCES

- Adão, T., Hruška, J., Pádua, L., Bessa, J., Peres, E., Morais, R., ... Sousa, J. J. (2017). Hyperspectral Imaging: A Review on UAV-Based Sensors, Data Processing and Applications for Agriculture and Forestry. *Remote Sensing*, 9(11), 1110. <https://doi.org/10.3390/rs9111110>
- Adeel, Z., Safriel, U., Niemeijer, D., & White, R. (2005). Ecosystems and human well-being: Desertification synthesis. Millennium Ecosystem Assessment. *World Resources Institute, Washington, DC*.
- Anderson, K. E., Glenn, N. F., Spaete, L. P., Shinneman, D. J., Pilliod, D. S., Arkle, R. S., ... Derryberry, D. W. R. (2018). Estimating vegetation biomass and cover across large plots in shrub and grass dominated drylands using terrestrial lidar and machine learning. *Ecological Indicators*. <https://doi.org/10.1016/j.ecolind.2017.09.034>
- Arora, V. (2002). Modeling vegetation as a dynamic component in soil-vegetation-atmosphere transfer schemes and hydrological models. *Reviews of Geophysics*, 40(2), 1006. <https://doi.org/10.1029/2001RG000103>
- Baena, S., Moat, J., Whaley, O., & Boyd, D. S. (2017). Identifying species from the air: UAVs and the very high resolution challenge for plant conservation. *PLoS ONE*, 12(11), 1–21. <https://doi.org/10.1371/journal.pone.0188714>
- Baret, F., & Guyot, G. (1991). Potentials and limits of vegetation indices for LAI and APAR assessment. *Remote sensing of environment*, 35(2-3), 161-173.
- Benz, U. C., Hofmann, P., Willhauck, G., Lingenfelder, I., & Heynen, M. (2004). Multi-resolution, object-oriented fuzzy analysis of remote sensing data for GIS-ready information. *ISPRS Journal of Photogrammetry and Remote Sensing*, 58(3–4), 239–258. <https://doi.org/10.1016/j.isprsjprs.2003.10.002>
- Bestelmeyer, B. T., Andrew Ash, Brown, J. R., Densambuu, B., Fernández-Giménez, M.,

- Johanson, J., ... Shaver, P. (2017). *Rangeland Systems. Rangeland Systems, processes, Management and challenges*. <https://doi.org/10.1007/978-3-319-46709-2>
- Breckenridge, R. P., & Dakins, M. E. (2011). Evaluation of Bare Ground on Rangelands Using Unmanned Aerial Vehicles: A Case Study. *GIScience & Remote Sensing*, 48(1), 74–85. <https://doi.org/10.2747/1548-1603.48.1.74>
- Breda, N. J. J. (2003). Ground-based measurements of leaf area index: a review of methods, instruments and current controversies. *Journal of Experimental Botany*, 54(392), 2403–2417. <https://doi.org/10.1093/jxb/erg263>
- Bukowski, B. E., & Baker, W. L. (2013). Historical fire regimes, reconstructed from land-survey data, led to complexity and fluctuation in sagebrush landscapes. *Ecological Applications*, 23(3), 546–564. <https://doi.org/10.1890/12-0844.1>
- Cagney, J., Cox, S. E., & Booth, D. T. (2011). Comparison of point intercept and image analysis for monitoring rangeland transects. *Rangeland Ecology and Management*, 64(3), 309–315. <https://doi.org/10.2111/REM-D-10-00090.1>
- Chen, B., Huang, B., & Xu, B. (2017). Multi-source remotely sensed data fusion for improving land cover classification. *ISPRS Journal of Photogrammetry and Remote Sensing*, 124, 27–39. <https://doi.org/10.1016/j.isprsjprs.2016.12.008>
- Chen, J., Yi, S., Qin, Y., & Wang, X. (2016). Improving estimates of fractional vegetation cover based on UAV in alpine grassland on the Qinghai–Tibetan Plateau. *International Journal of Remote Sensing*, 37(8), 1922–1936. <https://doi.org/10.1080/01431161.2016.1165884>
- Clark, P. E., & Seyfried, M. S. (2001). Point Sampling for Leaf Area Index in Sagebrush Steppe Communities. *Journal of Range Management*, 54(5), 589. <https://doi.org/10.2307/4003589>
- Cleveland, C. C., Reed, S. C., Keller, A. B., Nemergut, D. R., O’Neill, S. P., Ostertag, R., & Vitousek, P. M. (2014). Litter quality versus soil microbial community controls over decomposition: a quantitative analysis. *Oecologia*, 174(1), 283–294. <https://doi.org/10.1007/s00442-013-2758-9>
- Coble, A. A., & Hart, S. C. (2013). The significance of atmospheric nutrient inputs and

- canopy interception of precipitation during ecosystem development in piñon–juniper woodlands of the southwestern USA. *Journal of Arid Environments*, 98, 79–87.  
<https://doi.org/10.1016/j.jaridenv.2013.08.002>
- Cunliffe, A., & Anderson, K. (2019). Measuring Above-ground Biomass with Drone Photogrammetry: Data Collection Protocol. *Protocol Exchange*, 1–22.  
<https://doi.org/10.1038/protex.2018.134>
- Cunliffe, A. M., Brazier, R. E., & Anderson, K. (2016). Ultra-fine grain landscape-scale quantification of dryland vegetation structure with drone-acquired structure-from-motion photogrammetry. *Remote Sensing of Environment*, 183, 129–143.  
<https://doi.org/10.1016/j.rse.2016.05.019>
- Dashti, H., Poley, A., Glenn, N. F., Ilangakoon, N., Spaete, L., Roberts, D., ... Mitchell, J. J. (2019). Regional scale dryland vegetation classification with an integrated lidar-hyperspectral approach. *Remote Sensing*, 11(18). <https://doi.org/10.3390/rs11182141>
- Davies, A. G. M., Bakker, J. D., Dunwiddie, P. W., Hall, S. A., Downs, J., Evans, J., ... Evans, J. (2016). Trajectories of change in sagebrush steppe vegetation communities in relation to multiple wildfires. *Source: Ecological Applications Ecological Applications*, 22(5), 1562–1577. Retrieved from  
<http://www.jstor.org/stable/41722874>
- Davies, K. W., Boyd, C. S., Beck, J. L., Bates, J. D., Svejcar, T. J., & Gregg, M. A. (2011). Saving the sagebrush sea: An ecosystem conservation plan for big sagebrush plant communities. *Biological Conservation*, 144(11), 2573–2584.  
<https://doi.org/10.1016/j.biocon.2011.07.016>
- de Graaff, M.-A., Throop, H. L., Verburg, P. S. J., Arnone, J. A., & Campos, X. (2014). A Synthesis of Climate and Vegetation Cover Effects on Biogeochemical Cycling in Shrub-Dominated Drylands. *Ecosystems*, 17(5), 931–945.  
<https://doi.org/10.1007/s10021-014-9764-6>
- De Luca, G., N. Silva, J. M., Cerasoli, S., Araújo, J., Campos, J., Di Fazio, S., & Modica, G. (2019). Object-Based Land Cover Classification of Cork Oak Woodlands using UAV Imagery and Orfeo ToolBox. *Remote Sensing*, 11(10), 1238.

<https://doi.org/10.3390/rs11101238>

- de Roo, A. P. J., Wesseling, C. G., & Ritsema, C. J. (1996). A Single-Event Physically Based Hydrological and Soil Erosion Model for Drainage Basins. I: Theory, Input, and Output. *Hydrological Processes*, *10*(8), 1119–1126.  
[https://doi.org/10.1002/\(SICI\)1099-1085\(199608\)10:8<1119::AID-HYP416>3.0.CO;2-V](https://doi.org/10.1002/(SICI)1099-1085(199608)10:8<1119::AID-HYP416>3.0.CO;2-V)
- Dudley, K. L., Dennison, P. E., Roth, K. L., Roberts, D. A., & Coates, A. R. (2015). A multi-temporal spectral library approach for mapping vegetation species across spatial and temporal phenological gradients. *Remote Sensing of Environment*, *167*, 121–134. <https://doi.org/10.1016/j.rse.2015.05.004>
- Fern, R. R., Foxley, E. A., Bruno, A., & Morrison, M. L. (2018). Suitability of NDVI and OSAVI as estimators of green biomass and coverage in a semi-arid rangeland. *Ecological Indicators*, *94*(May), 16–21.  
<https://doi.org/10.1016/j.ecolind.2018.06.029>
- Flerchinger, G. N., Fellows, A. W., Seyfried, M. S., Clark, P. E., & Lohse, K. A. (2019). Water and Carbon Fluxes Along an Elevational Gradient in a Sagebrush Ecosystem. *Ecosystems*. <https://doi.org/10.1007/s10021-019-00400-x>
- Forsmo, J., Anderson, K., Macleod, C. J. A., Wilkinson, M. E., & Brazier, R. (2018). Drone- based structure- from- motion photogrammetry captures grassland sward height variability. *Journal of Applied Ecology*, *55*(6), 2587–2599.  
<https://doi.org/10.1111/1365-2664.13148>
- Gholizadeh, H., Gamon, J. A., Zyguelbaum, A. I., Wang, R., Schweiger, A. K., & Cavender-Bares, J. (2018). Remote sensing of biodiversity: Soil correction and data dimension reduction methods improve assessment of  $\alpha$ -diversity (species richness) in prairie ecosystems. *Remote Sensing of Environment*, *206*(November 2017), 240–253. <https://doi.org/10.1016/j.rse.2017.12.014>
- Gillan, J. K., Karl, J. W., Duniway, M., & Elaksher, A. (2014). Modeling vegetation heights from high resolution stereo aerial photography: An application for broad-scale rangeland monitoring. *Journal of Environmental Management*, *144*, 226–235.

<https://doi.org/10.1016/j.jenvman.2014.05.028>

- Gitelson, A. A., Kaufman, Y. J., & Merzlyak, M. N. (1996). Use of a green channel in remote sensing of global vegetation from EOS- MODIS. *Remote Sensing of Environment*, 58(3), 289–298. [https://doi.org/10.1016/S0034-4257\(96\)00072-7](https://doi.org/10.1016/S0034-4257(96)00072-7)
- Goodrich B, Gabry J, Ali I, Brilleman S (2020). “rstanarm: Bayesian applied regression modeling via Stan.” R package version 2.19.3, <https://mc-stan.org/rstanarm>.
- Gu, Y., Hunt, E., Wardlow, B., Basara, J. B., Brown, J. F., & Verdin, J. P. (2008). Evaluation of MODIS NDVI and NDWI for vegetation drought monitoring using Oklahoma Mesonet soil moisture data. *Geophysical Research Letters*, 35(22), L22401. <https://doi.org/10.1029/2008GL035772>
- Hamner, B. & Frasco, M. (2018). Metrics: Evaluation Metrics for Machine Learning. R package version 0.1.4. <https://CRAN.R-project.org/package=Metrics>
- Hann, W. J., Jones, J. L., Keane, R. E., Hessburg, P. F., & Gravenmier, R. A. (1998). Landscape dynamics. *Journal of Forestry*, 96(10), 10–15. <https://doi.org/10.1093/jof/96.10.10>
- Hay, G. J., & Castilla, G. (2006). Geographic Object-Based Image Analysis (GEOBIA): A new name for a new discipline. In *Object-Based Image Analysis* (Vol. 36, pp. 75–89). Berlin, Heidelberg: Springer Berlin Heidelberg. [https://doi.org/10.1007/978-3-540-77058-9\\_4](https://doi.org/10.1007/978-3-540-77058-9_4)
- Hillman, S., Wallace, L., Reinke, K., Hally, B., Jones, S., & Saldias, D. S. (2019). A Method for Validating the Structural Completeness of Understory Vegetation Models Captured with 3D Remote Sensing. *Remote Sensing*, 11(18), 2118. <https://doi.org/10.3390/rs11182118>
- Homer, C. G., Aldridge, C. L., Meyer, D. K., & Schell, S. J. (2012). Multi-scale remote sensing sagebrush characterization with regression trees over Wyoming, USA: Laying a foundation for monitoring. *International Journal of Applied Earth Observation and Geoinformation*, 14(1), 233–244. <https://doi.org/10.1016/j.jag.2011.09.012>
- Horning, N., Robinson, J. A., Sterling, E. J., Turner, W., & Spector, S. (2010). *Remote*

*sensing for ecology and conservation: a handbook of techniques*. Oxford University Press.

- Hossain, M. D., & Chen, D. (2019). Segmentation for Object-Based Image Analysis (OBIA): A review of algorithms and challenges from remote sensing perspective. *ISPRS Journal of Photogrammetry and Remote Sensing*, *150*, 115–134. <https://doi.org/10.1016/j.isprsjprs.2019.02.009>
- Howell, R. G., Jensen, R. R., Petersen, S. L., & Larsen, R. T. (2020). Measuring Height Characteristics of Sagebrush (*Artemisia* sp.) Using Imagery Derived from Small Unmanned Aerial Systems (sUAS). *Drones*, *4*(1), 6. <https://doi.org/10.3390/drones4010006>
- Husson, E., Reese, H., & Ecke, F. (2017). Combining Spectral Data and a DSM from UAS-Images for Improved Classification of Non-Submerged Aquatic Vegetation. *Remote Sensing*, *9*(3), 247. <https://doi.org/10.3390/rs9030247>
- Jiapaer, G., Chen, X., & Bao, A. (2011). A comparison of methods for estimating fractional vegetation cover in arid regions. *Agricultural and Forest Meteorology*, *151*(12), 1698–1710. <https://doi.org/10.1016/j.agrformet.2011.07.004>
- Jones, M. O., Allred, B. W., Naugle, D. E., Maestas, J. D., Donnelly, P., Metz, L. J., ... McIver, J. D. (2018). Innovation in rangeland monitoring: annual, 30 m, plant functional type percent cover maps for U.S. rangelands, 1984-2017. *Ecosphere*, *9*(9), e02430. <https://doi.org/10.1002/ecs2.2430>
- Karl, J. W., & Maurer, B. A. (2010). Multivariate correlations between imagery and field measurements across scales: comparing pixel aggregation and image segmentation. *Landscape Ecology*, *25*(4), 591–605. <https://doi.org/10.1007/s10980-009-9439-4>
- Kattenborn, T., Eichel, J., Wisler, S., Burrows, L., Fassnacht, F. E., & Schmidtlein, S. (2020). Convolutional Neural Networks accurately predict cover fractions of plant species and communities in Unmanned Aerial Vehicle imagery. *Remote Sensing in Ecology and Conservation*, rse2.146. <https://doi.org/10.1002/rse2.146>
- Knapp, P. A. (1996). Cheatgrass (*Bromus tectorum* L) Dominance in the Great Basin Desert and Influences. *Global Environmental Change*, *6*(1), 37–52.

- Komárek, J., Klouček, T., & Prošek, J. (2018). The potential of Unmanned Aerial Systems: A tool towards precision classification of hard-to-distinguish vegetation types? *International Journal of Applied Earth Observation and Geoinformation*, *71*, 9–19. <https://doi.org/10.1016/j.jag.2018.05.003>
- Lehnert, L. W., Meyer, H., Wang, Y., Mieke, G., Thies, B., Reudenbach, C., & Bendix, J. (2015). Retrieval of grassland plant coverage on the Tibetan Plateau based on a multi-scale, multi-sensor and multi-method approach. *Remote Sensing of Environment*, *164*, 197–207. <https://doi.org/10.1016/j.rse.2015.04.020>
- Leitão, P. J., & Santos, M. J. (2019). Improving Models of Species Ecological Niches: A Remote Sensing Overview. *Frontiers in Ecology and Evolution*, *7*, 9. <https://doi.org/10.3389/fevo.2019.00009>
- Leprieur, C., Kerr, Y. H., Mastorchio, S., & Meunier, J. C. (2000). Monitoring vegetation cover across semi-arid regions: Comparison of remote observations from various scales. *International Journal of Remote Sensing*, *21*(2), 281–300. <https://doi.org/10.1080/014311600210830>
- Liu, Q., Zhang, T., Li, Y., Li, Y., Bu, C., & Zhang, Q. (2019). Comparative Analysis of Fractional Vegetation Cover Estimation Based on Multi-sensor Data in a Semi-arid Sandy Area. *Chinese Geographical Science*, *29*(1), 166–180. <https://doi.org/10.1007/s11769-018-1010-2>
- López-Urrutia, Angel (2013). "Macroscopic Patterns in Marine Plankton" in *Encyclopedia of Biodiversity* (0-12-384720-6, 978-0-12-384720-1), (p. 667).
- Lu, M., Chen, B., Liao, X., Yue, T., Yue, H., Ren, S., ... Xu, B. (2017). Forest Types Classification Based on Multi-Source Data Fusion. *Remote Sensing*, *9*(11), 1153. <https://doi.org/10.3390/rs9111153>
- Maestre, F. T., Quero, J. L., Gotelli, N. J., Escudero, A., Ochoa, V., Delgado-Baquerizo, M., ... Zaady, E. (2012). Plant Species Richness and Ecosystem Multifunctionality in Global Drylands. *Science*, *335*(6065), 214 LP – 218. <https://doi.org/10.1126/science.1215442>
- Marticorena, B., Bergametti, G., Gillette, D., & Belnap, J. (1997). Factors controlling

- threshold friction velocity in semiarid and arid areas of the United States. *Journal of Geophysical Research: Atmospheres*, 102(D19), 23277–23287.
- McFeeters S. K. (1996) The use of the Normalized Difference Water Index (NDWI) in the delineation of open water features, *International Journal of Remote Sensing*, 17:7, 1425-1432, DOI: 10.1080/01431169608948714
- McGwire, K. C., Weltz, M. A., Finzel, J. A., Morris, C. E., Fenstermaker, L. F., & McGraw, D. S. (2013). Multiscale assessment of green leaf cover in a semi-arid rangeland with a small unmanned aerial vehicle. *International Journal of Remote Sensing*, 34(5), 1615–1632. <https://doi.org/10.1080/01431161.2012.723836>
- Mu, Q., Heinsch, F. A., Zhao, M., & Running, S. W. (2007). Regional evaporation estimates from flux tower and MODIS satellite data. *Remote Sensing of Environment*, 106(3), 285–304. <https://doi.org/10.1016/j.rse.2006.07.007>
- Ochoa-Hueso, R., Eldridge, D. J., Delgado-Baquerizo, M., Soliveres, S., Bowker, M. A., Gross, N., ... Maestre, F. T. (2018). Soil fungal abundance and plant functional traits drive fertile island formation in global drylands. *Journal of Ecology*, 106(1), 242–253. <https://doi.org/10.1111/1365-2745.12871>
- Olsoy, P. J., Forbey, J. S., Rachlow, J. L., Nobler, J. D., Glenn, N. F., & Shipley, L. A. (2015). Fearscales: Mapping functional properties of cover for prey with terrestrial LiDAR. *BioScience*, 65(1), 74–80. <https://doi.org/10.1093/biosci/biu189>
- Olsoy, P. J., Mitchell, J. J., Levia, D. F., Clark, P. E., & Glenn, N. F. (2016). Estimation of big sagebrush leaf area index with terrestrial laser scanning. *Ecological Indicators*, 61, 815–821. <https://doi.org/10.1016/j.ecolind.2015.10.034>
- Olsoy, P. J., Shipley, L. A., Rachlow, J. L., Forbey, J. S., Glenn, N. F., Burgess, M. A., & Thornton, D. H. (2018). Unmanned aerial systems measure structural habitat features for wildlife across multiple scales. *Methods in Ecology and Evolution*, 9(3), 594–604. <https://doi.org/10.1111/2041-210X.12919>
- Palace, M., Herrick, C., DelGreco, J., Finnell, D., Garnello, A., McCalley, C., ... Varner, R. (2018). Determining Subarctic Peatland Vegetation Using an Unmanned Aerial System (UAS). *Remote Sensing*, 10(9), 1498. <https://doi.org/10.3390/rs10091498>

- Pandit, K., Dashti, H., Glenn, N. F., Flores, A. N., Maguire, K. C., Shinneman, D. J., ... Fellows, A. W. (2018). Optimizing shrub parameters to estimate gross primary production of the sagebrush ecosystem using the Ecosystem Demography (EDv2.2) model. *Geoscientific Model Development Discussions*, (December), 1–23. <https://doi.org/https://doi.org/10.5194/gmd-2018-264>
- Peña-Barragán, J. M., Ngugi, M. K., Plant, R. E., & Six, J. (2011). Object-based crop identification using multiple vegetation indices, textural features and crop phenology. *Remote Sensing of Environment*, *115*(6), 1301–1316. <https://doi.org/10.1016/j.rse.2011.01.009>
- Poulter, B., Frank, D., Ciais, P., Myneni, R. B., Andela, N., Bi, J., ... Van Der Werf, G. R. (2014). Contribution of semi-arid ecosystems to interannual variability of the global carbon cycle. *Nature*, *509*(7502), 600–603. <https://doi.org/10.1038/nature13376>
- Prieto, I., Padilla, F. M., Armas, C., & Pugnaire, F. I. (2011). The role of hydraulic lift on seedling establishment under a nurse plant species in a semi-arid environment. *Perspectives in Plant Ecology, Evolution and Systematics*, *13*(3), 181–187. <https://doi.org/10.1016/j.ppees.2011.05.002>
- Prošek, J., & Šimová, P. (2019). UAV for mapping shrubland vegetation: Does fusion of spectral and vertical information derived from a single sensor increase the classification accuracy? *International Journal of Applied Earth Observation and Geoinformation*, *75*, 151–162. <https://doi.org/10.1016/j.jag.2018.10.009>
- Pyke, D. A., Chambers, J. C., Pellant, M., Knick, S. T., Miller, R. F., Beck, J. L., ... McIver, J. D. (2015). Restoration Handbook for Sagebrush Steppe Ecosystems with Emphasis on Greater Sage-Grouse Habitat— Part 1. Concepts for Understanding and Applying Restoration U.S. Geological Survey Circular 1416, 44. <https://doi.org/10.3133/circ1416>
- Qi, J., Chehbouni, A., Huete, A. R., Kerr, Y. H., & Sorooshian, S. (1994). A modify soil adjust vegetation index. *Remote Sensing of Environment*, *126*, 119–126. Retrieved from <https://pubag.nal.usda.gov/download/50306/PDF>

- Räsänen, A., Aurela, M., Juutinen, S., Kumpula, T., Lohila, A., Penttilä, T., & Virtanen, T. (2019). Detecting northern peatland vegetation patterns at ultra- high spatial resolution. *Remote Sensing in Ecology and Conservation*, rse2.140.  
<https://doi.org/10.1002/rse2.140>
- Räsänen, A., & Virtanen, T. (2019). Data and resolution requirements in mapping vegetation in spatially heterogeneous landscapes. *Remote Sensing of Environment*, 230, 111207. <https://doi.org/10.1016/j.rse.2019.05.026>
- Rasmussen, J., Ntakos, G., Nielsen, J., Svendsgaard, J., Poulsen, R. N., & Christensen, S. (2016). Are vegetation indices derived from consumer-grade cameras mounted on UAVs sufficiently reliable for assessing experimental plots? *European Journal of Agronomy*, 74, 75–92. <https://doi.org/10.1016/J.EJA.2015.11.026>
- Reisner, M. D., Grace, J. B., Pyke, D. A., & Doescher, P. S. (2013). Conditions favouring *Bromus tectorum* dominance of endangered sagebrush steppe ecosystems. *Journal of Applied Ecology*, 50(4), 1039–1049. <https://doi.org/10.1111/1365-2664.12097>
- Reynolds, J. F., Herrick, J. E., Huber-Sannwald, E., Jiang, H., Leemans, R., Lynam, T., ... Fernandez, R. J. (2007). Global Desertification: Building a Science for Dryland Development. *Science*, 316(5826), 847–851.  
<https://doi.org/10.1126/science.1131634>
- Rigge, M., Homer, C., Cleaves, L., Meyer, D. K., Bunde, B., Shi, H., ... Bobo, M. (2020). Quantifying Western U.S. Rangelands as Fractional Components with Multi-Resolution Remote Sensing and In Situ Data. *Remote Sensing*, 12(3), 412.  
<https://doi.org/10.3390/rs12030412>
- Rondeaux, G., Steven, M., & Baret, F. (1996). Optimization of soil-adjusted vegetation indices. *Remote Sensing of Environment*, 55(2), 95–107.  
[https://doi.org/10.1016/0034-4257\(95\)00186-7](https://doi.org/10.1016/0034-4257(95)00186-7)
- Rouse, J.W., Jr., Haas, R.H., Schell, J.A., & Deering, D.W. (1973). Monitoring the vernal advancement and retrogradation (green wave effect) of natural vegetation. *Prog. Rep. RSC 1978-1*. Remote Sensing Center, Texas A&M Univ., College Station.
- Saiz, H., Le Bagousse- Pinguet, Y., Gross, N., & Maestre, F. T. (2019). Intransitivity

- increases plant functional diversity by limiting dominance in drylands worldwide. *Journal of Ecology*, *107*(1), 240–252. <https://doi.org/10.1111/1365-2745.13018>
- Sankey, T. T., McVay, J., Swetnam, T. L., McClaran, M. P., Heilman, P., & Nichols, M. (2018). UAV hyperspectral and lidar data and their fusion for arid and semi-arid land vegetation monitoring. *Remote Sensing in Ecology and Conservation*, *4*(1), 20–33. <https://doi.org/10.1002/rse2.44>
- Schäfer, E., Heiskanen, J., Heikinheimo, V., & Pellikka, P. (2016). Mapping tree species diversity of a tropical montane forest by unsupervised clustering of airborne imaging spectroscopy data. *Ecological Indicators*, *64*, 49–58. <https://doi.org/10.1016/J.ECOLIND.2015.12.026>
- Schaffer, B. E., Nordbotten, J. M., & Rodriguez-Iturbe, I. (2015). Plant biomass and soil moisture dynamics: analytical results. *Proceedings of the Royal Society A: Mathematical, Physical and Engineering Sciences*, *471*(2183), 20150179. <https://doi.org/10.1098/rspa.2015.0179>
- Seaquist, J. ., Olsson, L., & Ardö, J. (2003). A remote sensing-based primary production model for grassland biomes. *Ecological Modelling*, *169*(1), 131–155. [https://doi.org/10.1016/S0304-3800\(03\)00267-9](https://doi.org/10.1016/S0304-3800(03)00267-9)
- Segoli, M., Ungar, E. D., Giladi, I., Arnon, A., & Shachak, M. (2012). Untangling the positive and negative effects of shrubs on herbaceous vegetation in drylands. *Landscape Ecology*, *27*(6), 899–910. <https://doi.org/10.1007/s10980-012-9736-1>
- Slaughter, C. W., Marks, D., Flerchinger, G. N., Van Vactor, S. S., & Burgess, M. (2001). Thirty-five years of research data collection at the Reynolds Creek Experimental Watershed, Idaho, United States. *Water Resources Research*, *37*(11), 2819–2823. <https://doi.org/10.1029/2001WR000413>
- Soudani, K., François, C., le Maire, G., Le Dantec, V., & Dufrêne, E. (2006). Comparative analysis of IKONOS, SPOT, and ETM+ data for leaf area index estimation in temperate coniferous and deciduous forest stands. *Remote Sensing of Environment*, *102*(1–2), 161–175. <https://doi.org/10.1016/j.rse.2006.02.004>
- Spaete, L. P., Glenn, N. F., & Baun, C. W. (2016). 2013 Morley Nelson Snake River

- Birds of Prey National Conservation Area RapidEye 7m Landcover Classification.
- Valencia, E., Maestre, F. T., Le Bagousse-Pinguet, Y., Quero, J. L., Tamme, R., Börger, L., ... Gross, N. (2015). Functional diversity enhances the resistance of ecosystem multifunctionality to aridity in Mediterranean drylands. *New Phytologist*, *206*(2), 660–671. <https://doi.org/10.1111/nph.13268>
- Wainwright, C. E., Davies, G. M., Dettweiler- Robinson, E., Dunwiddie, P. W., Wilderman, D., & Bakker, J. D. (2019). Methods for tracking sagebrush- steppe community trajectories and quantifying resilience in relation to disturbance and restoration. *Restoration Ecology*, *28*(1), 115–126. <https://doi.org/10.1111/rec.13060>
- Wang, X., Schaffer, B. E., Yang, Z., & Rodriguez-Iturbe, I. (2017). Probabilistic model predicts dynamics of vegetation biomass in a desert ecosystem in NW China. *Proceedings of the National Academy of Sciences*, *114*(25), E4944–E4950. <https://doi.org/10.1073/pnas.1703684114>
- White, M. A., Hoffman, F., Hargrove, W. W., & Nemani, R. R. (2005). A global framework for monitoring phenological responses to climate change. *Geophysical Research Letters*, *32*(4), 1–4. <https://doi.org/10.1029/2004GL021961>
- Woodward, F. I., & Cramer, W. (1996). Plant functional types and climatic changes : Introduction. *Journal of Vegetation Science*, *7*(3), 306–308.
- Xiao, J., Chevallier, F., Gomez, C., Guanter, L., Hicke, J. A., Huete, A. R., ... Zhang, X. (2019). Remote sensing of the terrestrial carbon cycle: A review of advances over 50 years. *Remote Sensing of Environment*, *233*, 111383. <https://doi.org/10.1016/j.rse.2019.111383>
- Zribi, M., Le Hégarat-Masclé, S., Taconet, O., Ciarletti, V., Vidal-Madjar, D., & Boussema, M. R. (2003). Derivation of wild vegetation cover density in semi-arid regions: ERS2/SAR evaluation. *International Journal of Remote Sensing*, *24*(6), 1335–1352. <https://doi.org/10.1080/01431160210146668>

## APPENDIX A

### **Comparison of Point Frame Data for Fractional Photosynthetic Cover**

We compared three methods of calculating photosynthetic cover or fractional vegetation cover from the point frame field data. The first method was reported in Chapter Two. This method divided all of the “green” hits per plot by the total hits per plot to calculate FPC – referred to as “All Hits”. The second method included only the first hits from the point frame pin drops; each plot has 100 pin drops, so the total of first green hits was always divided by 100. This is referred to as “First Hits”. Lastly, we tested a different metric: fractional vegetation cover (FVC). We calculated FVC by dividing all vegetation hits (green or not) and dividing by the total number of hits. We reviewed the mean absolute error (MAE), correlation value (Rho), and root mean square difference (RMSD), for each method tested against the estimated values of FPC. Results differed for each site.

At lowest site, we found that all comparisons between the point frame data and the estimated FPC did not co-vary and there was no relationship between the data types (Table A.1).

For LOS, we found that using only the first hits from the point frame data had the highest rho value (0.86) and lowest MAE and RMSD values (0.06 and 0.08, respectively). The estimated FPC from the UAS imagery also had significant positive correlation with the first hit calculations and FVC (Table A.1).

At the final site, MBS, we observed that the strongest correlation between estimated and field FPC occurred when using the all of the point frame data hits (rho = 0.55). However, the lowest RMSD and MAE values were seen when we tested the correlation between estimated FPC and FVC (Table A.1).

**Table A.1** Summary of field data correlations to estimated photosynthetic cover for each study site.

	WBS	LOS	MBS
<b>All Hits</b>			
AllHitMAE	0.25	0.18	0.31
AllHitRho	0.09	0.75	0.55
AllHitRMSD	0.32	0.20	0.36
<b>First Hits</b>			
FirstHitMAE	0.26	0.06	0.21
FirstHitRho	0.03	0.86	0.42
FirstHitRMSD	0.31	0.08	0.26
<b>Fractional Veg Cover</b>			
FVCMaE	0.18	0.13	0.15
FVCRho	0.07	0.68	0.46
FVCRMSD	0.23	0.15	0.18

## APPENDIX B

## Canopy Height Model from Multispectral Point Cloud

We used Cloud Compare and RStudio to create canopy height models (CHM) from multispectral point clouds. Outlined here are the steps used to create the product.

Input: dense multispectral point cloud from Agisoft. Clouds were not filtered in Agisoft. Exported from Agisoft in projected coordinate system: NAD 83 UTM Z 11 N. Export as .txt file to retain spectral data. Must be exported with 14 points of precision to retain all Z information.

Note: In cloud compare it's helpful to rename clouds as you go to keep track of progress.

1. Save a copy of the point cloud file to local drive.
2. Open in Cloud Compare.
3. Manually remove unwanted objects, ie: solar panel, flux tower, cars, etc.
4. Calculate NDVI for point cloud using scalar field calculator.
5. Switch view to NDVI and split point cloud using NDVI values/visual inspection of height with min/max tool (Record numeric value of NDVI used to split).
6. Grid the remaining ground cloud by .75m. Use min height values -- gridded cloud.
7. Compute Normals on gridded ground cloud: surface = triangulation; use preferred orientation = +Z.
8. Use Poisson surface tool to generate a mesh. Check "output surface density".
9. Trim mesh volume to surface using min/max split tool.
10. Smooth mesh with Laplacian function Sampling = 20. Smoothing factor = 0.200.
11. Sample the smoothed mesh with points. Density > 2,000 points. --> cloud ground surface.
12. Activate and select BOTH ground-surface cloud and the original, full NDVI point cloud. Trim the bounding box so that extent between both clouds is the same. For the next steps, use the trimmed clouds.
13. Rasterize and export the trimmed, ground-surface cloud at min height and desired resolution.
14. Rasterize and export the trimmed, NDVI cloud at max height and the SAME resolution as the ground surface.
15. Open RStudio.

16. Load the trimmed ground surface raster and the trimmed digital surface model (DSM). Subtract the ground raster from the DSM. The output is a CHM.

## APPENDIX C

### Segmentation Parameters

**Table C.1** Segmentation Parameters used for each site on the RGB imagery within the ArcGIS Pro segmentation tool.

	<b>Wyoming Big Sage</b>
Spectral Detail	18.5
Spatial Detail	15
Min Segment Size in Pixels	55
	<b>Low Sage</b>
Spectral Detail	17
Spatial Detail	15
Min Segment Size in Pixels	55
	<b>Mountain Big Sage</b>
Spectral Detail	15.5
Spatial Detail	15
Min Segment Size in Pixels	20